The temperature-dependent shear strength of ice-filled joints in rock mass considering the effect of joint roughness, opening and shear rates

Shibing Huang[1,2], Haowei Cai[1], Zekun Xin[1], Gang Liu[1]

[1] School of Resources and Environmental Engineering, Wuhan University of Science and Technology, Wuhan, Hubei 430081, China

[2] Hubei Key Laboratory for Efficient Utilization and Agglomeration of Metallurgic Mineral Resources, Wuhan University of Science and Technology, Wuhan, Hubei 430081, China

Correspondence to: Shibing Huang (huangshibing@wust.edu.cn)

Abstract. Global warming causes many rockfall activities of the alpine mountains, especially when ice-filled joints in the rock mass become thawed. The warming and thawing of frozen soils and intact rocks were widely studied in the past several decades, however, the variation of shear strengths of ice-filled joints was not fully understood. In this study, a series of compression-shear experiments were conducted to investigate the shear strength of ice-filled rock joints by considering the effects of joint roughness, temperature, opening, shear rates and normal stress. The joint roughness can improve the shear strength of ice-filled joints. However, the contribution of joint roughness is controlled by some noticeable bulges instead of the JRC index. The shear strength linearly increases with increasing the aggregation of rupture ice area before these noticeable bulges. As the joint opening increases, the effect of joint roughness decreases and the shear strength of ice-filled joints tends to be equal to the shear strength of pure ice. In addition, the shear strength quickly reduces with increasing temperature from -15 ℃ to -0.5 ℃. The

shear failure mode changes from shear cracking of joint ice to the shear debonding of ice-rock interface

above -1 °C. Increasing shear rate will decrease the shear strength of ice-filled joints because the joint

ice displays the brittle failure phenomenon at a high shear rate. The shear strength of ice-filled joints

linearly increases with increasing the normal stress. Moreover, it is also proved that the Mohr-coulomb

criterion can be used to characterize the shear strength of ice-filled joints under different normal stresses.

This research can provide a better understanding of the warming degradation mechanism of ice-filled

joints by considering the above important influencing factors.

1 Introduction

With the increase of global temperature and human activities in permafrost areas, many alpine rock

masses become more unstable (Gruber and Haeberli, 2007; Allen and Huggle, 2013; Hartmeyer et al.,

2020; Legay et al., 2021; Hilger et al., 2021). A large number of rockfalls in permafrost alpine bedrock

slopes indicated the exposure of broken ice after shear failure, which could cause serious natural

geological disasters (Krautblatter et al., 2021; Walter et al., 2019). For example, the rockfall disaster that

happened in Chamoli, Indian Himalaya, in 2021 took more than 200 lives and destroyed two hydropower

facilities (Shugar et al., 2021). According to investigation results, this rockfall disaster was caused by the

warming and thawing of ice. It is evidenced that a huge frost heaving pressure will be produced to drive

the voids and joints propagation and thus cause the instability of joint rock masses during the freezing

process (Huang et al., 2022a; 2022b). Fortunately, the bonding strength between ice and joint wall can

strengthen the joints themselves after complete freezing (Matsuoka and Murton, 2008; Zhang et al., 2020;

Shan et al., 2021; Wang et al., 2022). However, if the joint ice was thawed, the rock-ice-rock "sandwich"

structure would be debonded and unstable. In addition, the liquid water produced by warming ice could

42   lower the friction between joint surface and thus reduced the stability of joint rock slopes (Zhao et al.,

43   2017). Many field data showed that most of the irreversible fracture displacement and rockfall happened

44   in the warm seasons instead of the cool seasons because the warming and thawing of joint ice could

45   greatly decrease the strength of rock mass containing ice-filled joints (Weber et al., 2018; Etzelmüller et

46   al., 2022). Yang et al. (2019) claimed that the existence of detached ice block could promote the mobility

47   of ice-rock system and thus cause a more serious geological disaster on alpine rock slope. Therefore, the

48   warming degradation of the ice-rock interface and the strength loss of ice-filled joints should be

49   comprehensively studied.

50   In the past decades, the warming degradation of permafrost soils was widely investigated, however, there

51   is little literature reporting the strength loss of rocks containing ice-filled joints. The shear experiment of

52   the ice-rock interface might be first conducted by replacing the rock with concrete in order to make a

53   specific roughness (Davies et al., 2001, 2017). These experiments were conducted at the temperature

54   from -5 to 0 °C. Krautblatter et al. (2012) developed a shear strength model for the ice-filled joints that

55   incorporates the cracking of rock bridges, the friction of rough joint walls, creep of ice and detachment

56   of rock-ice interfaces. Mamot et al. (2018) conducted a systematic study of the shear failure of limestone-

57   ice and mica-rich interfaces at constant strain rates from -10 to -0.5℃, and they found that the normal

58   stress and freezing temperature were two important factors influencing the shear strength. However, the

59   uniform joint surfaces were used without considering the influence of joint roughness. Mamot et al. (2021)

60   further predicted the warming stability of permafrost slopes containing ice-filled joints by using the

61   Universal Distinct Element Code (UDEC). The simulation results verified that the warming temperature

62   close to the melting point might drive the slide of a slope with angle of 50°-62°, and the actual slope

angle also depended on the joint orientation. The above research mainly investigated the thawing

temperature and normal stress on the shear strength of ice-filled joints. The highest normal stress is about

1.438 MPa (Davies et al., 2001), and the maximum range for the temperature was -10 ℃ to -0.5 ℃

(Mamot et al., 2018). However, the freezing depth could exceed 100 m for some alpine caves containing

frozen ice (normal stress large than 2 MPa) and the temperature was less than -15 ℃ as observed in the

field (Colucci and Guglielmin, 2019). Therefore, a much wider range of temperature should be

considered when investigating the shear characteristics of ice-filled joints.

In addition, although some scholars began to pay attention to the mechanical properties of ice-filled joint

rock mass, the influence of many important factors on the shear strength of ice-filled joints was not

investigated, including the joint roughness, shear rate, normal stress and joint opening. Generally, the

natural joints have different roughness and openings (Shen et al., 2020). In this study, a comprehensive

shear experiment was performed on the ice-filled joints in sandstones. The main purpose was to reveal

the influencing mechanism of freezing temperature, joint roughness, shear rate, joint opening and normal

stress on the shear strength of ice-filled joints in rock masses. This research can provide a better

understanding of the warming degradation process of the ice-filled joints and the thawing disaster of

alpine mountains in cold regions.

2 Materials and methods

2.1 Collection of sandstones

The red sandstones collected from Yichang city of Hubei province were used in this experiment. This is

a typical sedimentary rock and is widely distributed on the surface of the earth. The block samples with

approximately equal P-wave (compressional wave) velocities were chosen to make frozen samples

containing ice-filled joints. The basic physico-mechanical properties of this red sandstone are given in

Table 1.

Table 1. The basic physico-mechanical properties of the fresh sandstone.

Density (ρ) (g/cm^3)	Porosity n (%)	Primary wave velocity V_p (m/s)		Shear strength τ_{ps} (MPa)		Uniaxial compressive strength UCS (MPa)	
		Dry	Saturated	Dry	Saturated	Dry	Saturated
2.32	7.71	2992	3264	7.60	3.02	79.53	30.97

2.2 Preparation of ice-filled joint rock mass

According to the JRC index proposed by Barton and Choubey (1977), five kinds of roughness were used

in this experiment, including No. 2 (2°-4°), No. 4 (6°-8°), No. 6 (10°-12°), No. 8 (14°-16°) and No. 10

(18°-20°), respectively. The frozen samples containing ice-filled joints are made in the laboratory

because it is hard to cut or drill them in the fields. The manufacturing process of ice-filled joint rock mass

mainly includes the following steps:

① The original rock blocks were cut into the designed rectangular blocks (100 mm × 100 mm × 50

mm) by using a rock cutting machine.

② These rectangular blocks were used to engrave different rough curves on the surface by using a 3D

numerical control engraving machine. The roughness can be controlled by implanting the standard JRC

curves into the controlling system of this machine. Each frozen rock sample containing an ice-filled joint

was assembled by using a pair of rectangular blocks with the same roughness.

100 ③ The rock blocks were heated in a dry oven at 105 ℃ in order to tightly paste the waterproof tape

101 and prevent the escape of joint water during freezing.

102 ④ The joint opening was divided into different specified thicknesses which were controlled by

103 inserting rubber strips, and a piece of waterproof tape was pasted on the surface in order to store water.

104 ⑤ When the waterproof tape was tightly bonded on the rock surface, liquid water should be injected

105 into the artificial joint until no water leaks out. After that, the water-filled joint rock mass was put into a

106 steel mold to freeze in a freezing chamber. The steel mold was used to control the joint opening because

107 the volume of joint water would expand during freezing. Then ice-filled joint samples can be derived

108 after freezing at -20 ℃ for 12 h. The manufacturing procedure and related ice-filled joint samples were

109 shown in Fig. 1.

110 **Table 2.** Ten standard joint profiles (Barton and Choubey, 1977).

Profile No.	Typical roughness profiles	JRC range
No. 1		0-2(0.4)
No. 2		2-4(2.8)
No. 3		4-6(5.8)
No. 4		6-8(6.7)
No. 5		8-10(9.5)
No. 6		10-12(10.8)
No. 7		12-14(12.8)

No. 8		14-16(14.5)
No. 9		16-18(16.7)
No. 10		18-20(18.7)

111
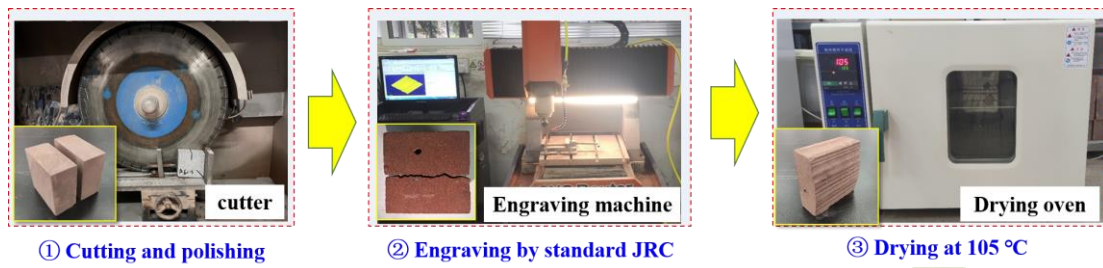
113 **Figure 1.** Preparation of ice-filled joints. The preparation steps are as follows: ① Cutting and polishing, ②

114 Engraving by standard, ③ Drying at 105 ℃, ④ Sealing joints up, ⑤ Injecting water and freezing.
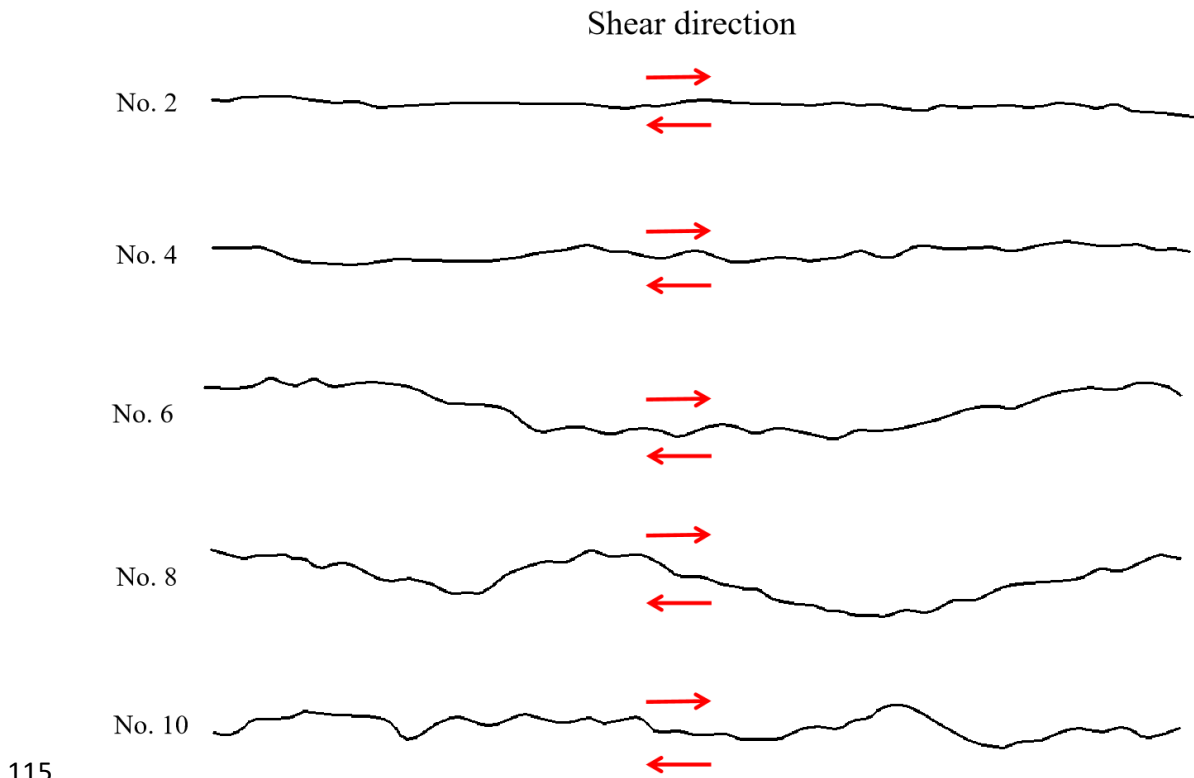
Figure 2. The shear directions for different joint profiles.

2.3 Experimental procedures

The main objective of this study is to investigate the effect of critical factors on the shear strength of ice-filled joint rock mass, including the freezing temperature, joint roughness, shear rates, joint opening and normal stress. The joint roughness is a basic index for rock joints, which is always considered when investigating other factors. Therefore, all the samples can be divided into 4 groups, namely the temperature group, shear rate group, joint opening group, and normal stress group. In the pre-test, the shear strength of the ice-filled joint does not change when the temperature is below -5 ℃, however, it greatly decreases when the temperature increases from -5 ℃ to 0 ℃. Therefore, the temperatures are set as -15 ℃, -5 ℃, -1 ℃ and -0.5 ℃, respectively. The shear rates are 0.2 mm/min, 0.4 mm/min and 0.8 mm/min in the shear rate group. In the joint opening group, the openings of ice-filled joints are 2 mm, 8

127 mm and 14 mm, respectively. The freezing depth on the earth may be small, however, it can exceed 100

128 m in some alpine caves, where the in-situ stress is close to 2 MPa. Therefore, in the normal stress group,

129 the normal stresses are set as 0 MPa, 0.5 MPa, 1 MPa, 1.5 MPa and 2 MPa, respectively. Three parallel

130 experiments were performed on each group to eliminate the discreteness of ice-filled joint samples and

131 experiment error. There are approximately 225 ice-filled joint samples prepared in this experiment. The

132 distribution of these ice-filled joint samples were shown in Fig. 3.

133 All the water-containing joints were frozen in a freeze box at a specific temperature for about 12 h, and

134 they were used to conduct the direct shear experiment on a temperature-controlled shearing instrument

135 under the scheduled low temperature and normal stress (Fig. 4). A temperature sensor was implanted into

136 the sample to accurately monitor the internal temperature change of ice-filled joint samples. In order to

137 adjust the height of the ice-filled samples, a steel sheet was placed between the indenter and joint blocks.

138 When the scheduled freezing temperature was reached, the normal stress was applied with a loading rate

139 of 0.2 kN/s. Then the shear process was performed in the displacement mode with the designed shear

140 rate. After the shear experiment, the rupture modes of ice-filled joints were captured and analyzed by

141 using a camera.

142
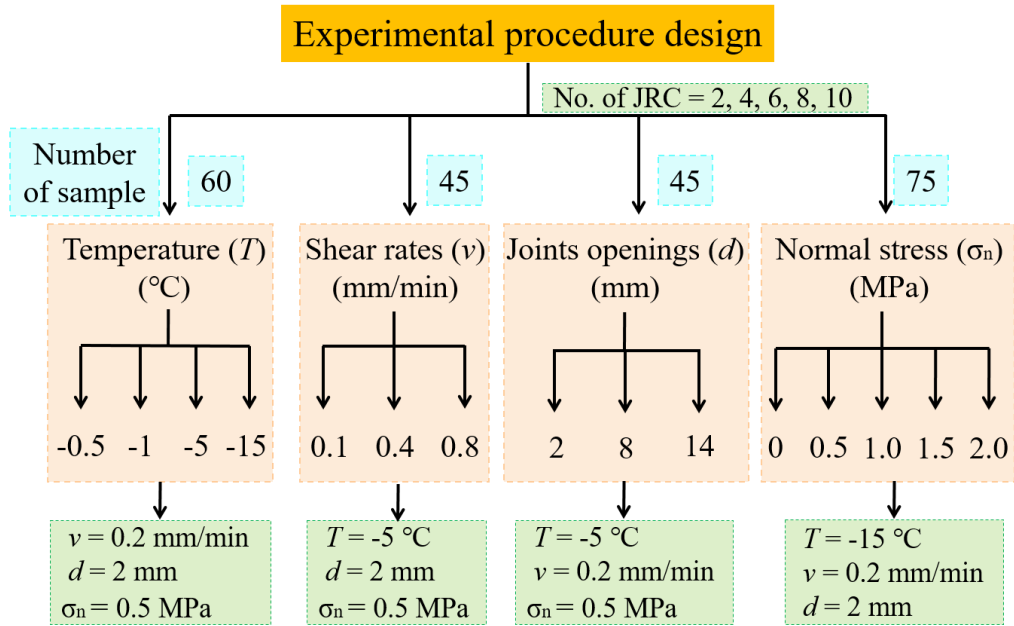
Figure 3. Distribution of rock samples containing ice-filled joints. T: Temperature. v: Shear rates. d: Joint openings.

143

σ_n: Normal stress.

144

145
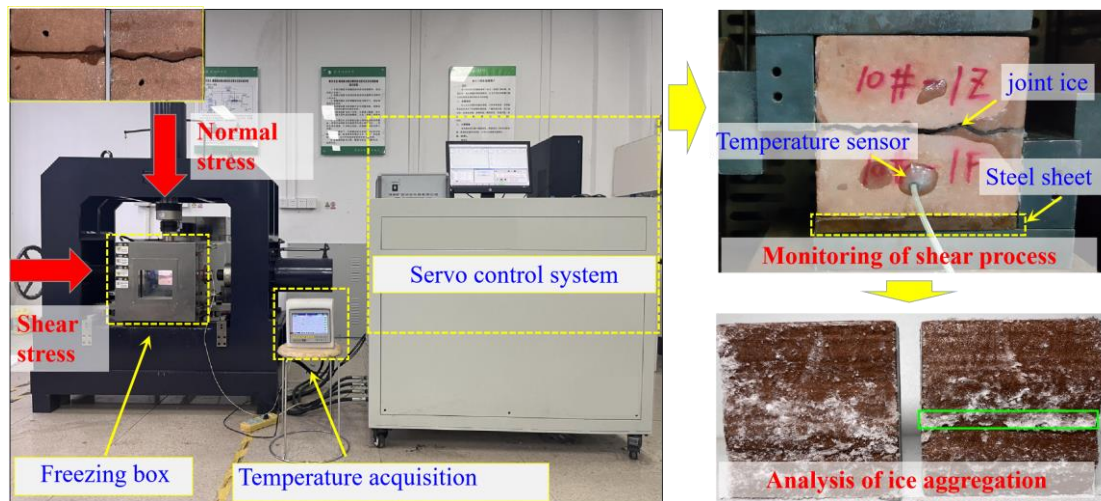
Figure 4. Shear experiment procedure and equipment

146

147   **3 Experimental results**

148   **3.1 Effect of freezing temperature and joint roughness**

149   In the temperature group, freezing temperatures were set as -15 ℃, -5 ℃, -1 ℃ and -0.5 ℃, and the joint

150   roughness was named by the profile number in Table 2. The shear strength is dependent on the freezing

151   temperature and joint roughness as shown in Fig. 5. The shear strength decreases remarkably with

152   increasing freezing temperature. When the temperature increases from -15 ℃ to -0.5 ℃, the mean

153   strength decreases by approximately 54%, 32%, 60%, 46% and 56% for profiles of No. 2, No. 4, No. 6,

154   No. 8 and No. 10, respectively. The shear strength of ice-filled joints does not always increase with JRC,

155   which has a considerable reduction at the joint profiles of No. 6 and No. 10. It illustrates that solid ice is

156   a kind of special infilled material, which is different from soft soils or cement-based materials (Xu et al.

157   2012; Zhao et al. 2020). The change trend of shear strength against JRC may be explained by the shear

158   rupture mode, as shown in Fig. 6a. There are several aggregation regions of rupture ice close to large

159   climbing bulges on the surface of joints. The peak shear strength of ice-filled joints is related to the

160   aggregation area of rupture ice, because a large shear force is required to promote the solid ice to shear

161   slide along the slope of bulges. It should be noted that the rupture ice has a white appearance, low

162   transparency and obvious rupture characteristics by observing the enlarged pictures of the ice-filled joints

163   after shear failure. Only the rupture ice before the noticeable bulges displays aggregation behavior. The

164   area of the aggregation ice can be calculated after estimating the width of the aggregation ice from the

165   pictures (Fig. 6b), because the joints are two-dimensional surfaces. This is a simple and approximate

166   estimation method for the aggregation area of rupture ice.

167   The accumulated aggregation area percentage of the rupture ice can be calculated as

168
$$A_i = \frac{\sum_{k=1}^{n} L_k}{L_{\text{joint}}} \times 100\% \tag{1}$$

169   where L_k is the width of the aggregation ice for the bulge k. $L_{\text{joint}} = 10$ cm, which is the trace length of the

170   joint.

171   The aggregation area and location along the rough profile of joints after shear failure are plotted in Fig.

172   7. It can be observed that the aggregation ice appears before several high bulges and the aggregation

173   location is almost independent of the freezing temperature if aggregation ice occurs. The climbing bulges

174   in front of the aggregation ice are noticeable and influential. It implies that the influence of joint

175   roughness on the shear strengths of these ice-filled joints may be only controlled by several noticeable

176   bulges instead of the JRC index. Figure 8 shows that the shear strengths of No. 6 and No. 10 display

177   obvious reduction trends, which may be in accordance with the ice aggregation area. The ice aggregation

178   area decreases with increasing the freezing temperature, because the bonding strength between ice and

179   joint surface becomes to be weaker, and the shear rupture happens along the ice-rock interface instead of

180   solid ice when the freezing temperature is larger than -0.5 ℃.

181   In addition, when the freezing temperature is close to 0 ℃, the pre-melting of ice-rock interface induced

182   by the normal stress will cause a reduction of bonding strength. Therefore, the shear strength between

183   bonded ice-rock interfaces is much smaller than the shear strength of solid ice at a high freezing

184   temperature close to the melting point of bulk ice, such as -0.5 ℃. It should be noted that the aggregation

185   phenomenon of rupture ice disappears when $T = -0.5$ ℃ because the high-temperature ice is ductile failure

186   along the ice-rock interface instead of the joint ice itself. However, the climbing effect still makes a

187   significant contribution to the increase of shear strength.

188
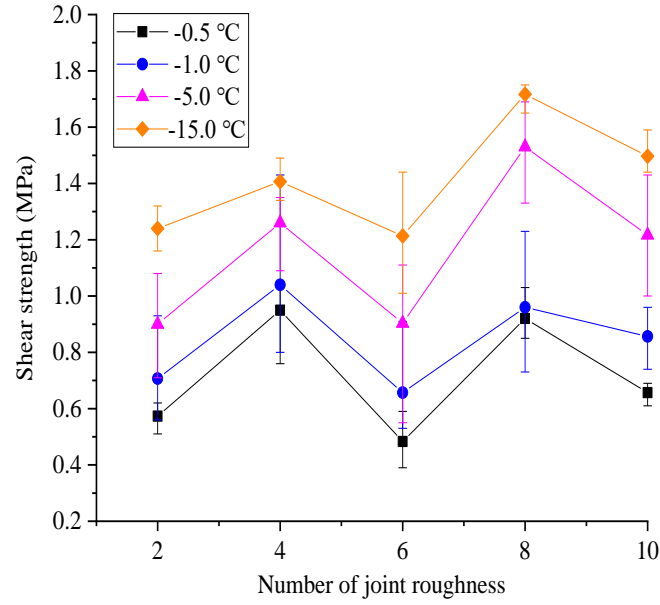
Figure 5. Shear strength against joint roughness at different freezing temperatures. Experimental condition: $v = 0.2$

190   mm/min, $d = 2$ mm, $\sigma_n = 0.5$ MPa.
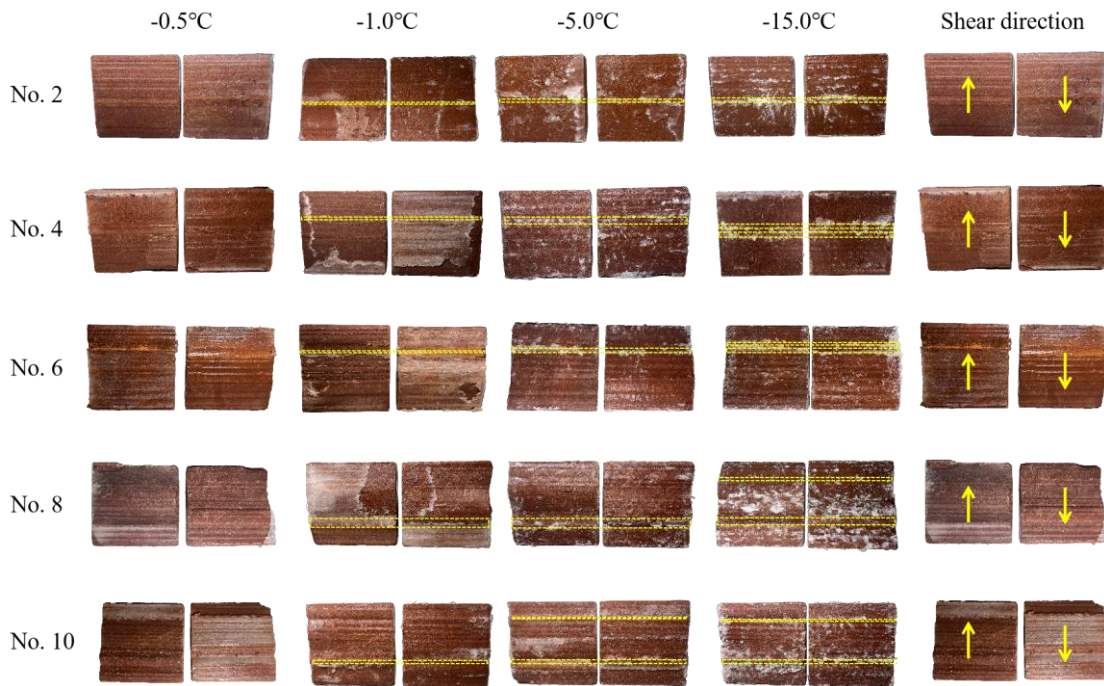
191

192   (a) Shear rupture modes
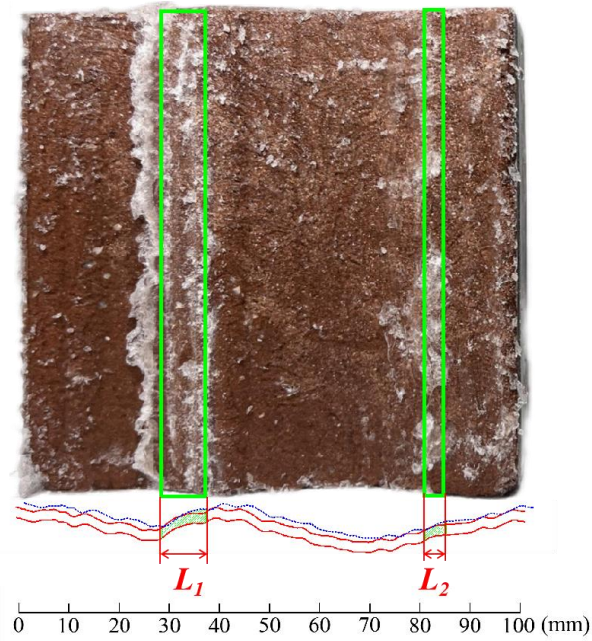
193

194   (b) Determination of the aggregation area of the rupture ice

195   **Figure 6.** Shear rupture modes and aggregation area of ice-filled joints at different freezing temperatures. The yellow
196   dotted lines show the main aggregation of rupture ice. Ice after rupture will aggregate in roughness bulges
197   perpendicular to the shear direction.

198

(b) No. 4

199

(c) No. 6

200

(d) No. 8

201

(e) No. 10
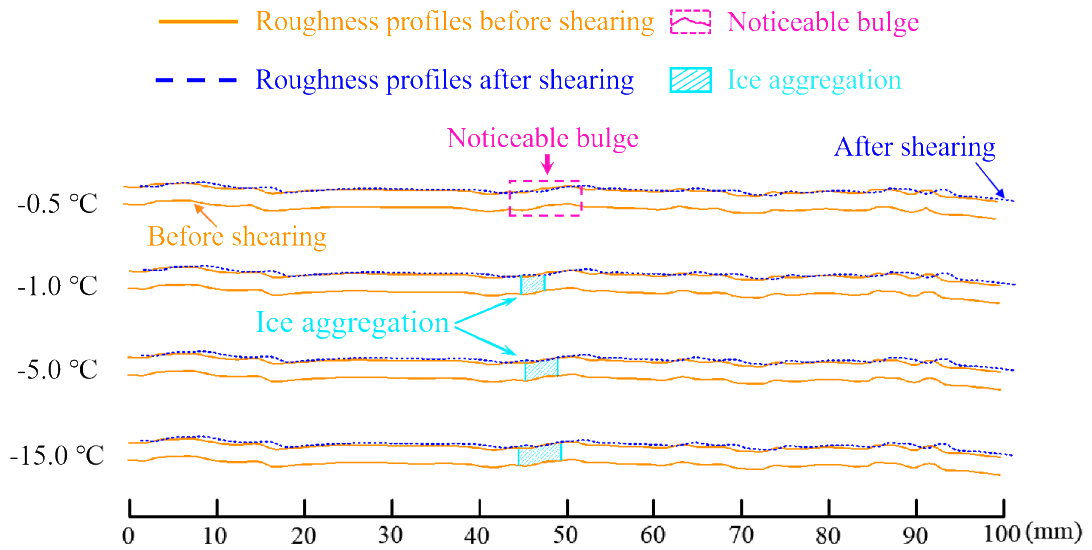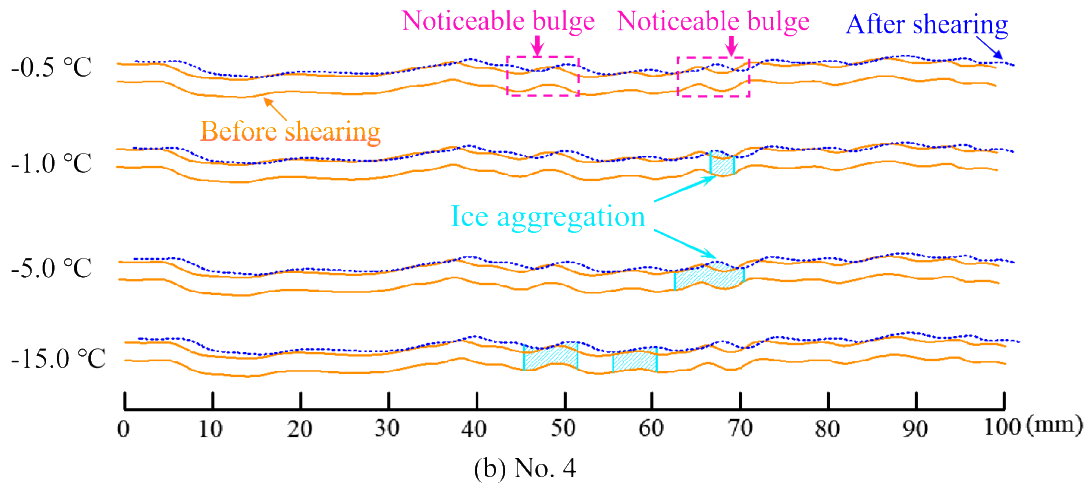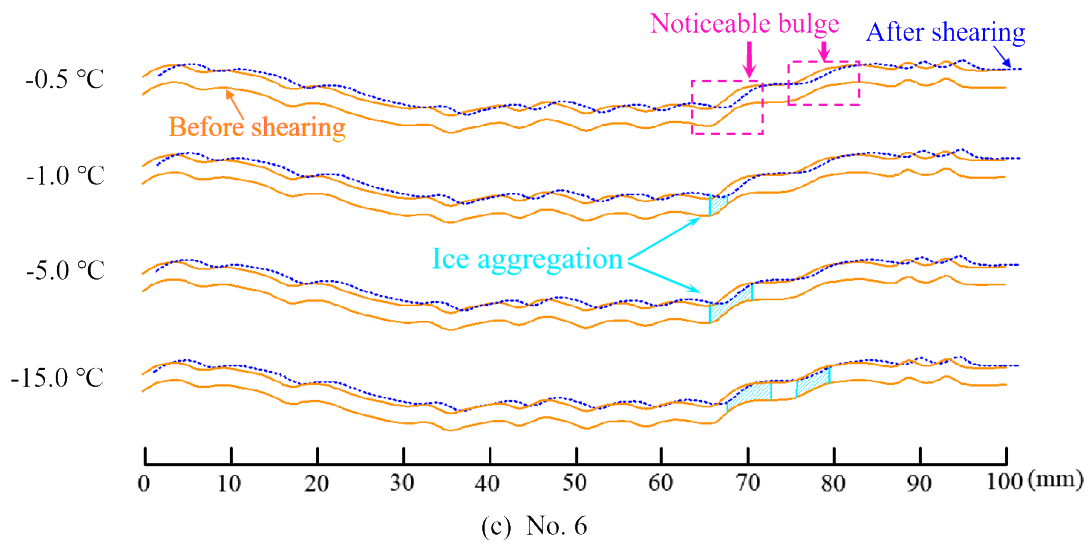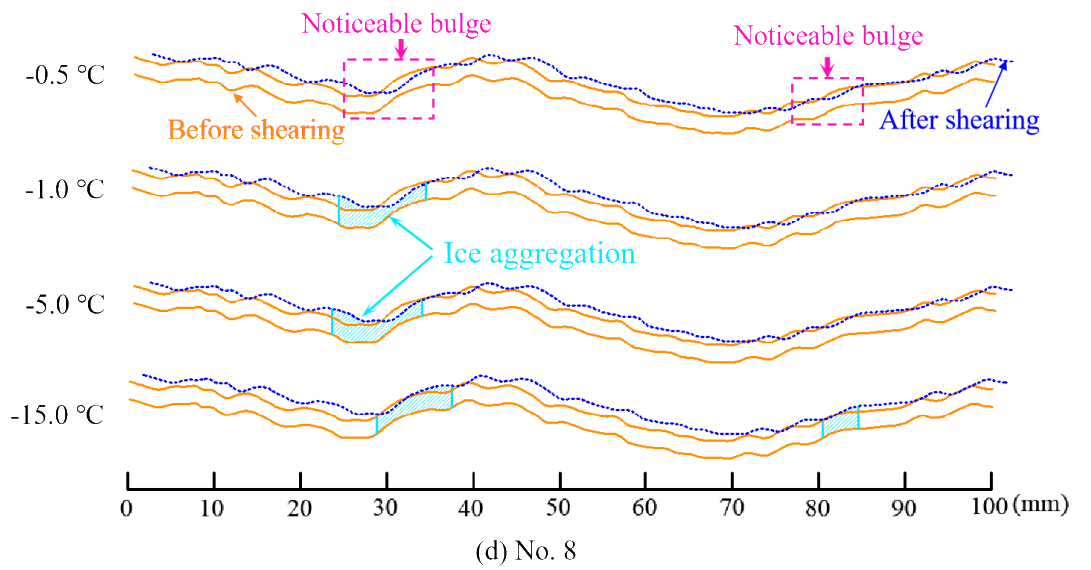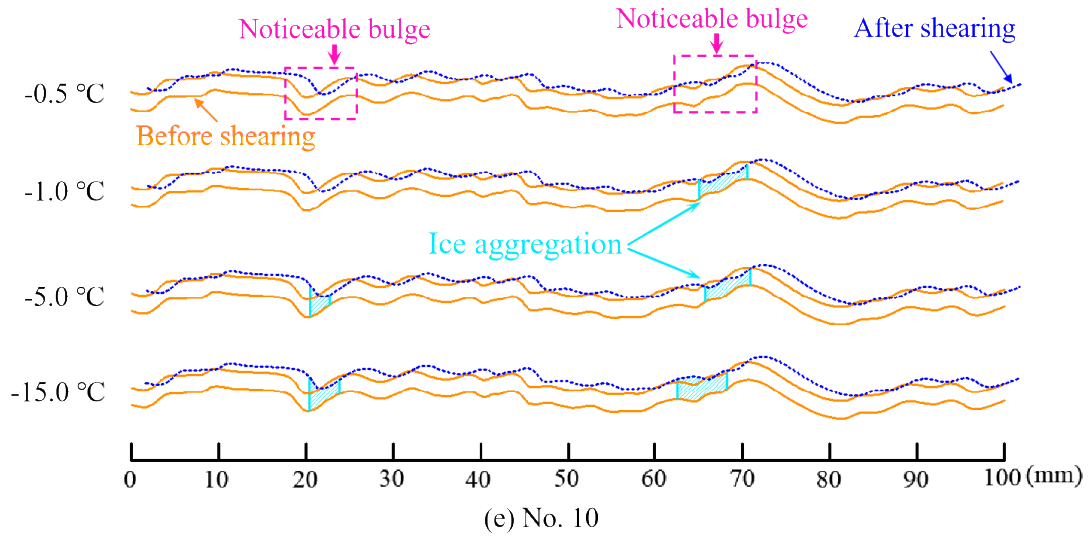
Figure 7. Shear aggregation areas of ice along the profile of roughness. Experimental condition: $v = 0.2$ mm/min, d = 2 mm, $\sigma_n = 0.5$ MPa. Some blue profiles (dotted curves) are located under the orange profiles (solid curves) after shearing, which means the width of joints becomes smaller. Generally, the reduction of joint width occurs before some bulges and the rupture ice will aggregate before these bulges. The bulges causing the reduction of joint width and aggregation of ice are called noticeable bulges. The noticeable bulges have larger inclination angles and they are far away from the joint edges.
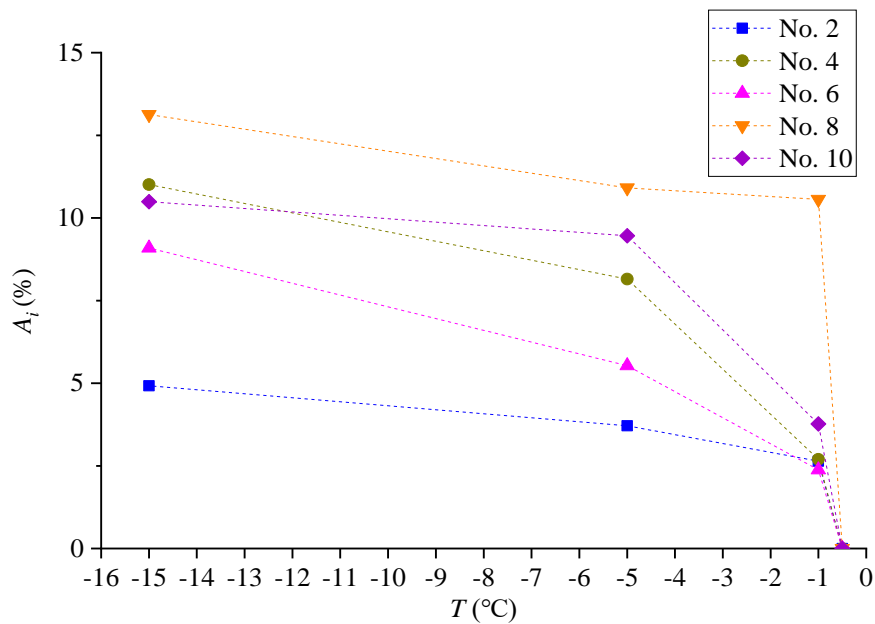
 Figure 8. Aggregation area of rupture ice increases with the reduction of freezing temperature. Experimental

211 conditions: $v = 0.2$ mm/min, $d = 2$ mm, $\sigma_n = 0.5$ MPa. A_i: aggregation area percentage of rupture ice.

212 The peak shear displacement and normal displacement also are dependent on the freezing temperature

213 (Table 3 and Table 4). With the increase of freezing temperature, the peak shear displacement increases

214 because the joint ice will change from brittle to ductile (Bragov et al., 2015). The brittle-ductile transition

215 of pure ice also is related to the freezing temperature, and the rupture ice will be produced under the

216 brittle failure condition. Lou et al. (2022) claimed that plain ice has strong brittleness at the temperature

217 from -5 °C to -20 °C. The increasing aggregation area of the rupture ice in Fig. 6 further proves that the

218 brittleness of ice increases with decreasing the freezing temperature. The maximum shear displacement

219 before failure is smaller at -15 °C, which may be caused by the high brittleness. When the temperature

220 increases to -1 °C, the solid ice becomes to be ductile, therefore a larger shear displacement arises before

221 failure. However, the shear dilatancy reduces with increasing the freezing temperature. Solid ice is a kind

222 of temperature-dependent material, the elastic modulus of which almost linearly decreases with

223 increasing freezing temperature (Sinha, 1989; Han et al. 2016). The inhibition of normal stress on the

224 shear dilatancy is greater at the high freezing temperature during the shear process.

225 Several typical shear stress-displacement and normal-shear displacement curves for the profile of No. 4

226 are plotted in Fig. 9. The ice-filled joint shows significant residual shear strength beyond the peak point,

227 which slightly decreases with increasing shear displacement. This residual shear strength is caused by

228 the friction effect between the upper and lower ice-filled blocks. In addition, the normal shear dilatancy

229 displays increasing trend with shear displacement, which is caused by the climbing effect of ice-filled

230 joints. It should be noted that the shear strength has a second rising point at the residual strength stage,

231 because the shear rate is increased from 0.2 mm/min to 1 mm/min in order to accelerate the completion

232 of the shear process. Schulson and Fortt (2012) claimed that the friction between ice interfaces increases

233 when the shear rates increase from 0.06 mm/min to 0.6 mm/min. Therefore, the sudden rise of residual

234 shear strength can be attributed to the accelerated shear rate.

235 **Table 3.** The peak shear displacement at the peak points of shear strength (mm)

Profile No.	Freezing temperature			
	-15 ℃	-5 ℃	-1 ℃	-0.5 ℃
No. 2	1.36	1.46	1.72	1.84
No. 4	1.62	1.75	1.86	2.08
No. 6	1.33	1.53	1.71	1.83
No. 8	1.78	1.85	1.99	2.12
No. 10	1.63	1.79	1.87	1.94

236

237 **Table 4.** The normal shear dilatancy at the point of peak shear strength (mm)

Profile No.	Freezing temperature			
	-15 ℃	-5 ℃	-1 ℃	-0.5 ℃
No. 2	0.24	0.23	0.14	0.08
No. 4	0.46	0.37	0.31	0.31
No. 6	0.27	0.28	0.22	0.12
No. 8	0.77	0.44	0.37	0.36
No. 10	0.61	0.32	0.21	0.39

238

239

240
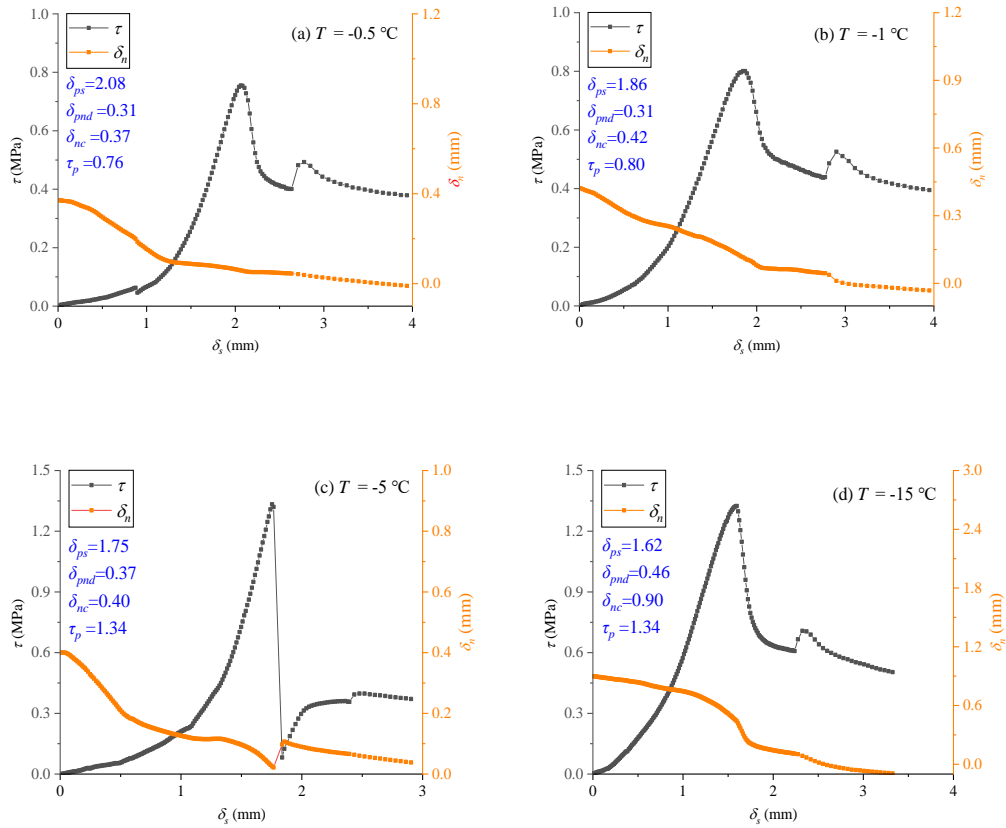
Figure 9. Shear strength and normal displacement versus the shear displacement for the profile of No. 4 in the

temperature group. δ_{ps} and δ_{pnd} are the shear displacement and normal shear dilatancy at the point of peak shear

strength, τ_p and δ_{nc} is the initial compression deformation.

Another finding is that the JRC is not suitable to interpret the influence of joint roughness on the shear

strength of ice-filled joints, because the peak shear strength does not monotonically increase with

increasing JRC index. The peak shear strength displays an increase-decrease-increase-decrease trend

against JRC from No. 2 to No. 10 (Fig. 5). Figure 10 shows that the peak shear strength displays a linear

increasing trend with increasing aggregation areas of fragmented ice after failure. The aggregation area

of fragmented ice can be treated as the effective climbing area which makes a significant contribution to

the improvement of shear strength, because the fragmented ice is produced under compression-shear

251 stress in the process of climbing the steep bulges. As a consequence, only these steep bulges causing

252 aggregation of rupture ice contribute to the improvement of shear strength. The variation law of shear

253 dilatancy against the roughness also is in accordance with the shear strength of ice-filled joints, but it is

254 different from the change law of JRC (Table 4). In Fig. 7, the gathering of fragmented ice mainly arises

255 in the front of the steepest bulge. It illustrates that the improvement of shear strength of joint ice is caused

256 by a part of the steepest bulge instead of the total roughness. Therefore, JCR may be not suitable for the

257 prediction of shear strength of ice-filled joints. For example, although the JCR of No. 6 is much larger

258 than No. 4, the effective steep bulge to cause ice aggregation after failure is smaller than that of No. 4

259 (Fig. 8). This phenomenon confirms that the improvement of shear strength is only caused by some

260 noticeable steep bulges instead of the total bulges.
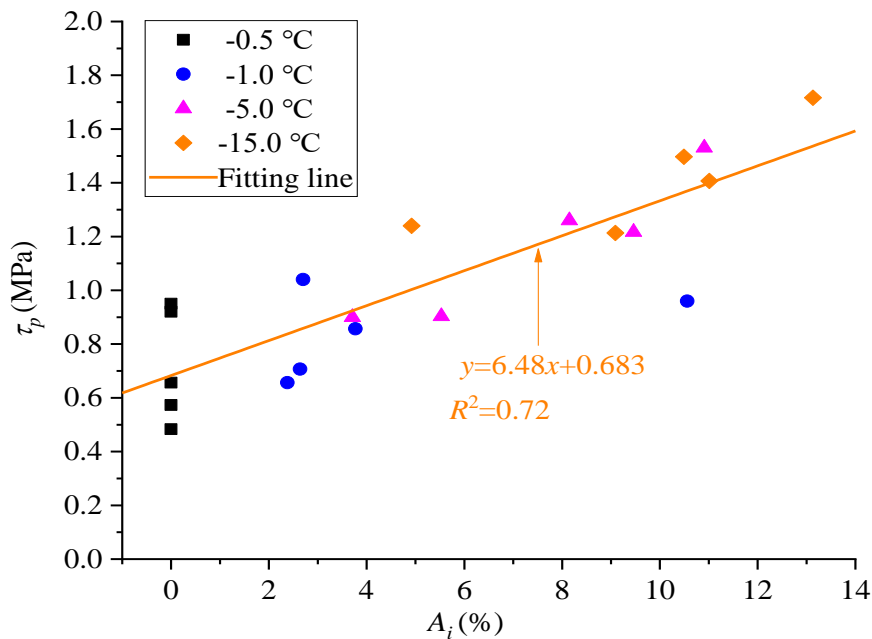
261

262 **Figure 10.** Peak shear strength linearly increases with increasing aggregation areas of rupture ice. Experimental

263 condition: v = 0.2 mm/min, d = 2 mm and σ_n = 0.5 MPa.

3.2 Effect of shear rates

The shear rates have significant effects on the strength of solid ice as observed in the previous literature (Petrovic, 2003). Low shear rates are used to conduct quasi-static shear experiments, including 0.2 mm/min, 0.4 mm/min and 0.8 mm/min. Figure 11 shows that the peak shear strength slightly decreases with increasing shear rates. Solid ice is a kind of typical elasto-plastic material. When the shear rate is slow, the ice crystal has enough time to shear slip and it will present ductile failure characteristics. At a low shear rate, the free water on the slip interface will reorganize at the water-ice interface to form ice, however, it is hard for the ice crystal to adjust to adapt the shear slip at high shear rates, which will cause the shear rupture of ice crystals and hinder the growth of ice on the water-ice interface (Luo et al., 2019). Mamot et al. (2018) claimed that a high strain rate of $10^{-3}\,\mathrm{s}^{-1}$ can induce brittle failure of ice and rock-ice contacts. At a lower shear rate, the stress concentration inside infilled ice can be relaxed and it changes to ductile creep deformation. Fukuzawa and Narita (1993) held that the brittle-ductile transition of ice under the shear process occurs around the strain rate of $10^{-4}\,\mathrm{s}^{-1}$. Here, the shear displacement rate is from 0.2 mm/min to 0.8 mm/min, corresponding to the strain rates from $1.67 \times 10^{-3}\,\mathrm{s}^{-1}$ to $6.67 \times 10^{-3}\,\mathrm{s}^{-1}$. Therefore, the shear rate in this study is very close to the threshold of brittle-ductile transition given in the previous literature. Figure 12 shows that a high shear rate will induce brittle failure of joint ice and more fragmented ice crystals are produced. As a result, the shear strength reduces with increasing shear rates from 0.2 mm/min to 0.8mm/min. In this study, the exact shear rate for the brittle and ductile transition of ice-filled joints is not accurately determined due to the limitation of the shear rate range. More further shear experiments should be carried out on the ice and ice-filled joints by adopting a larger range of the shear rate.
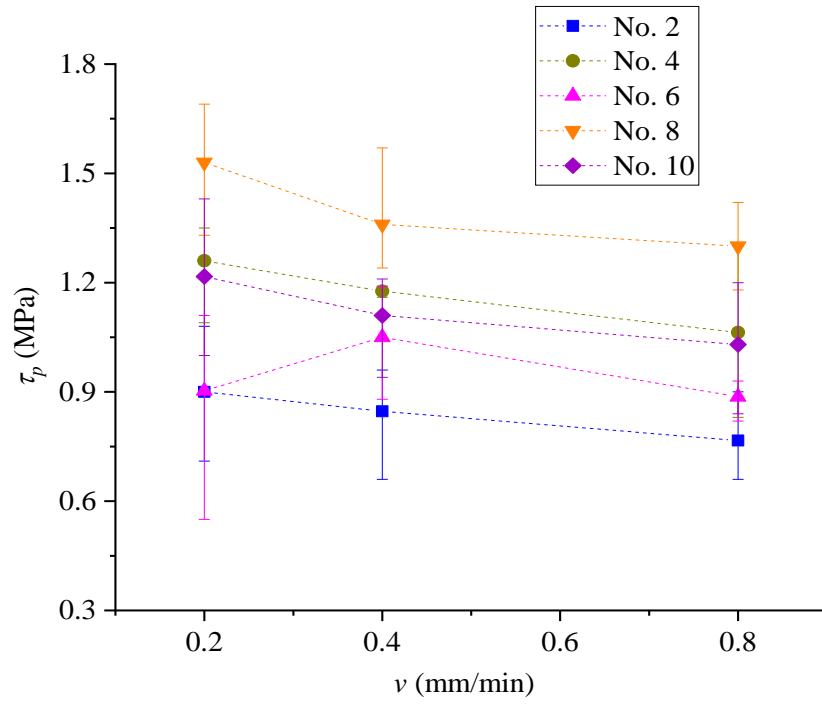
285

286 **Figure 11.** Effect of shear rate on the peak shear strength. Experimental condition: $T = -5$ °C, $d = 2$ mm and $\sigma_n = 0.5$

287 MPa.

288
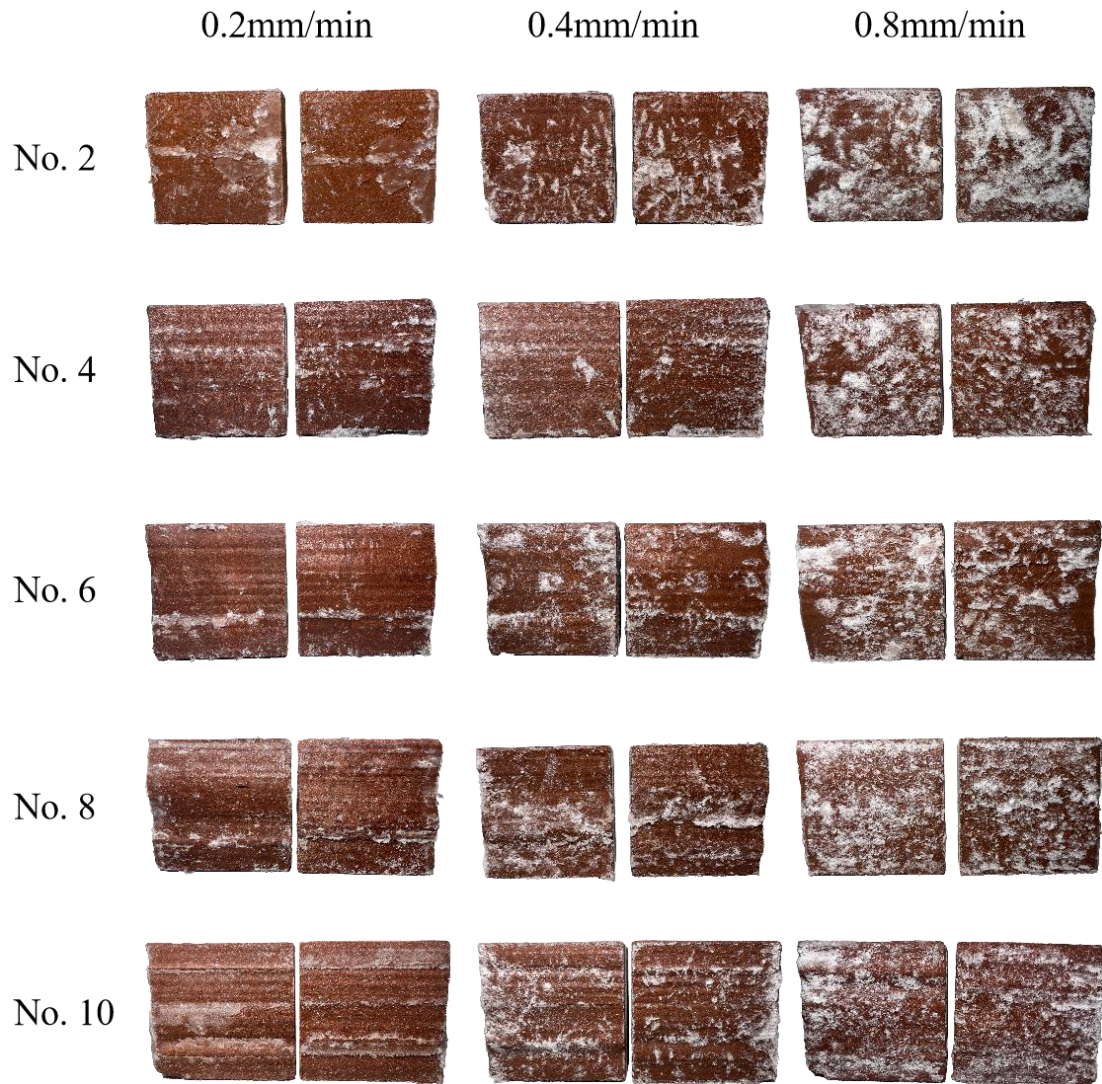
Figure 12. The shear rupture characteristics of joint ice under different shear rates. Experimental condition: $T = -5\,°C$, $d = 2$ mm and $\sigma_n = 0.5$ MPa. The ice crystal that cannot adapt to shear slip at high shear rates will form brittle failure. The joint ice of brittle failure shows more micro fractures which make it more reflective. This will cause a white appearance of the rupture ice on the joint surface. The ductile failure of ice displays a transparent appearance without white color, which is hard to observe. Therefore, a larger area of white appearance implies a much more serious brittle failure of joint ice.

3.4 Effect of joint openings

Joint opening is another critical factor influencing the shear strength of ice-filled joints, which is defined as the vertical distance between the upper and lower blocks. The standard JRC curves are suggested by Barton and Choubey (1977). We tested the maximum height difference of the standard JRC curves is approximately 2.14 mm, 2.40 mm, 6.24 mm, 6.85 mm and 4.48 mm for the profiles of No. 2, No. 4, No. 6, No. 8 and No. 10, respectively. The joint openings are chosen as 2 mm, 8 mm and 14 mm, because 2 mm is smaller than all the maximum height differences while 14 mm is much larger than them. The rupture characteristics of joint ice against the joint opening are plotted in Fig. 13. When the joint opening is 2 mm, the aggregation phenomenon of rupture ice is evident. However, the aggregation phenomenon disappears for the profiles of No. 2, No. 4 and No. 6 when the joint opening is 8 mm. When the joint opening increases to 14 mm, there is not any aggregation of rupture ice arising for all the joints. Figure 14 shows that when the joint opening increases from 2 mm to 14 mm, the shear strength of ice-filled joints decreases. The shear strength of pure solid ice also is measured in the laboratory, which is approximately 0.83 MPa on the condition that $T = -5$ °C, $v = 0.2$ mm/min and $\sigma_n = 0.5$ MPa. When the joint opening is 14 mm, the shear strengths of ice-filled joint are approximately 0.83 MPa and they are independent of the joint roughness. When the joint opening is 8 mm, the shear strengths of ice-filled joint are very close to the shear strength of pure solid ice (0.83 MPa) for the joint of No. 2, No. 4 and No. 6. The reason is that 8 mm has exceeded the critical filling thickness of these joints (No. 2, No. 4 and No. 6), therefore the shear strength of these ice-filled joints is only controlled by the solid ice instead of joint roughness. In addition, there is not any significant ice aggregation on the joint surfaces of No. 2, No. 4 and No. 6 when the joint opening is 8 mm, and the shear failure happens inside the joint ice. However,

317   for the ice-filled joints of No. 8 and No. 10, the shear strengths are larger than 0.83 MPa, which illustrates

318   that the critical filling thickness for the profiles of No. 8 and No. 10 should be larger than 8 mm but

319   smaller than 14 mm. There is aggregation ice arising before large bulges, and these large bulges would

320   prevent the direct shear failure of joint ice and improve the shear strength.

321   The influence of joint opening and roughness on the shear strength can be explained by using the shear

322   failure path of ice-filled joints as shown in Fig. 15. When d=2 mm, the shear climbing will occur before

323   some large bulges for all the joint profiles. This climbing action induces the aggregation of rupture ice

324   and change of shear path. As a consequence, the shear strength will improve. When d=8 mm, the shear

325   failure path will not be disturbed for the profiles of No. 2, No. 4 and No. 6, however, the shear failure

326   path changes due to the climbing action for the profiles of No. 8 and No. 10, in which a significant

327   aggregation of rupture ice is produced. Therefore, the shear strengths of ice-filled joints for the profiles

328   of No. 2, No. 4 and No. 6 are approximately equal to the solid ice, while the shear strengths for the

329   profiles of No. 8 and No. 10 are much larger than 0.83 MPa. When d = 14 mm, the shear failure happens

330   inside the joint ice for all joint profiles, therefore, the shear failure path and shear strength will not be

331   influenced by the joint roughness and no aggregation of rupture ice occurs. The shear dilatancy

332   deformation of the ice-filled joints in Fig. 16 has further proved the climbing actions, including all the

333   profiles with joint opening of 2 mm, and the profiles of No. 8 and No. 10 with joint opening of 8 mm.

334   The climbing effect of the No. 2 ice-filled joint with opening of 2 mm is not remarkable, therefore the

335   shear dilatancy is very small and the shear strength also is close to pure solid ice (0.83 MPa). Regardless

336   of the critical filling thickness, the present study shows that the shear strength of ice-filled joints

337   decreases with increasing joint openings from 2 mm to 14 mm, and it is related to the joint roughness

338 below the critical infilled thickness. When the filling ice exceeds the critical thickness, the shear strength

339 of ice-filled joints is equal to the shear strength of solid ice under the same condition. It should be noted

340 that the critical filling thickness for each roughness will be determined in future studies.

341
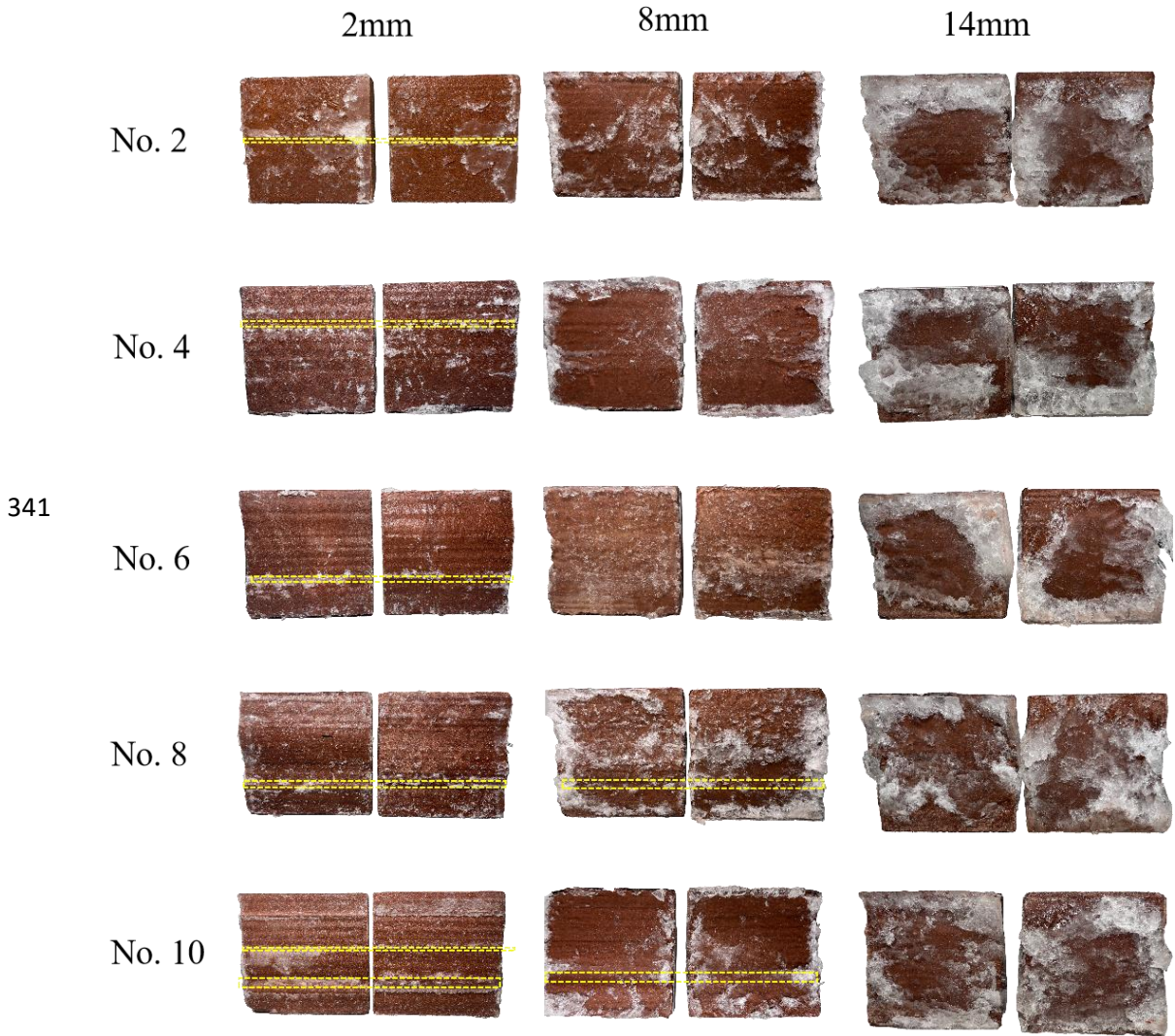
342 **Figure 13.** The shear rupture characteristics of ice-filled joints with different openings. Experimental condition: $T =$

343 -5 °C, $d = 2$ mm and $\sigma_n = 0.5$ MPa. The yellow lines show the main aggregation of rupture ice. Ice after rupture will

344 aggregate in roughness bulges perpendicular to the shear direction. The aggregation phenomenon disappears as the

345 joint openings increase. The aggregation phenomenon of profiles No. 2, No. 4 and No. 6 disappear in 8 mm joint

346 openings. All profiles' aggregation phenomena disappear in 14 mm joint openings.

347
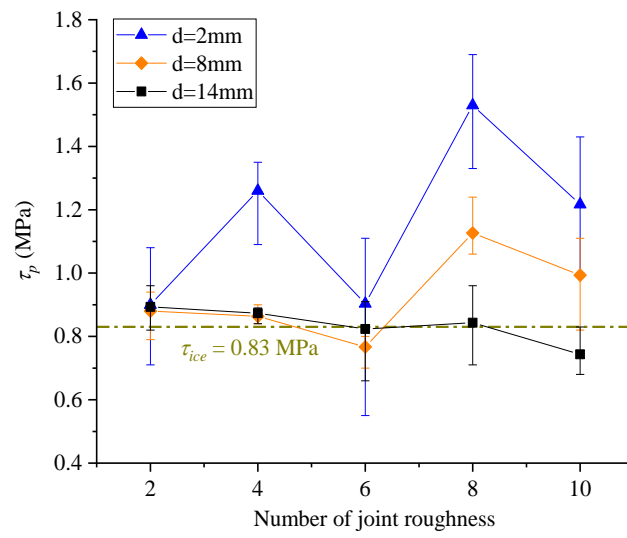
Figure 14. Effect of joint opening on the peak shear strength. Experimental condition: $T = $ -5 ℃, $v = 0.2$ mm/min

349   and $\sigma_n = 0.5$ MPa.

350
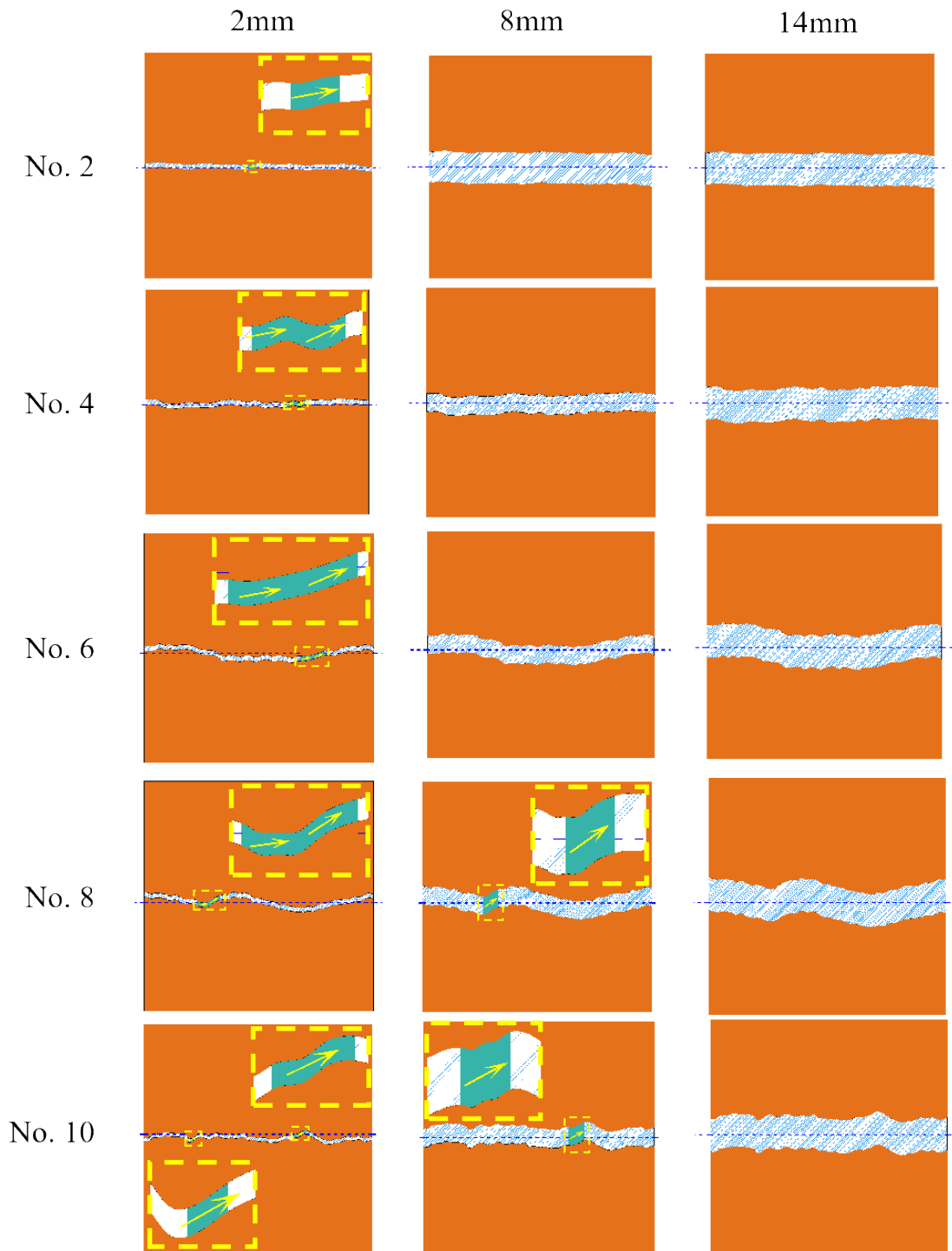
Figure 15. Influence of joint roughness on the shearing slip path. Experimental condition: T = -5 °C, v = 0.2 mm/min

and σ_n = 0.5 MPa.

353
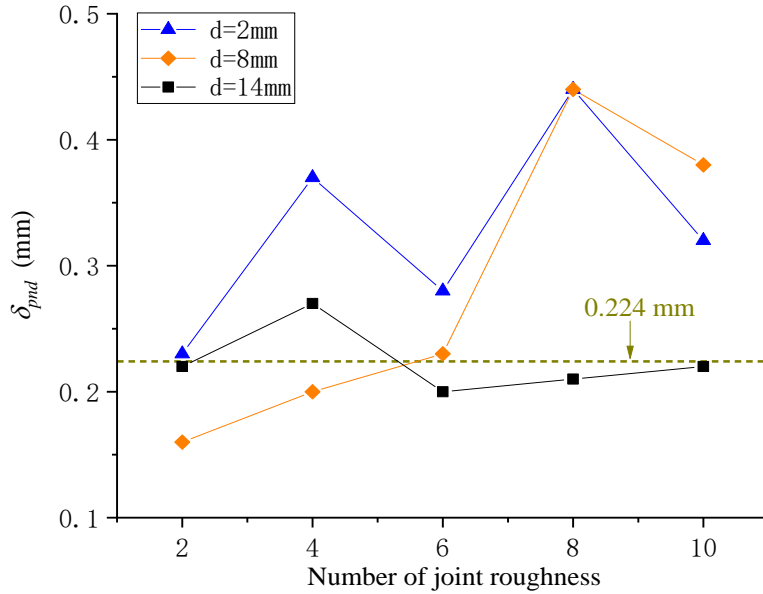
354

355   **Figure 16.** Effect of joint opening on the shearing dilatancy. Experimental condition: T = -5 °C, v = 0.2 mm/min and

356   σ_n = 0.5 MPa.

357   **3.5 Effect of normal stress**

358   The normal stress group was used to investigate the effect of normal stress on the shear strength of ice-

359   filled joints, including 0 MPa, 0.5 MPa, 1.0 MPa, 1.5 MPa and 2.0 MPa. The shear strength of ice-filled

360   joints displays a significant increasing trend with increasing normal stress (Fig. 17). The Mohr-coulomb

361   criterion may be used to express the relationship between the shear strength and normal stress as below:

362    $$\tau_p = c_j + \sigma_n \tan \phi_j \tag{2}$$

363   where τ_p = shear stress on plane, σ_n = normal stress on plane, c_j = cohesion of ice-filled joints,

364   ϕ_j = internal friction angle of ice-filled joints.

365   Figure 17 shows Mohr-coulomb criterion can be well used to calculate the shear strength of ice-filled

366   joints against the normal stress. The shear rupture modes of the joint ice are given in Fig. 18. A

367   remarkable ice aggregation phenomenon can be found on the surface of joints and the aggregation occurs

368 at a stable location of the joint profile regardless of the normal stress. The aggregation area of rupture ice

369 increases with increasing normal stress, because climbing bulges is harder and the solid ice is easier to

370 be crush at the front of large bulges under the higher normal stress (Fig. 19). In Section 3.1, it has

371 illustrated that the aggregation area of rupture ice is an important index to reflect the shear strength of

372 ice-filled joints at different freezing temperatures. Actually, the shear strength also linearly increases

373 with increasing the aggregation area of rupture ice under different normal stress as shown in Fig. 20. It

374 further illustrates that only some large bulges causing the aggregation of rupture ice can contribute to the

375 improvement of shear strength instead of the total roughness index, such as JRC.

376
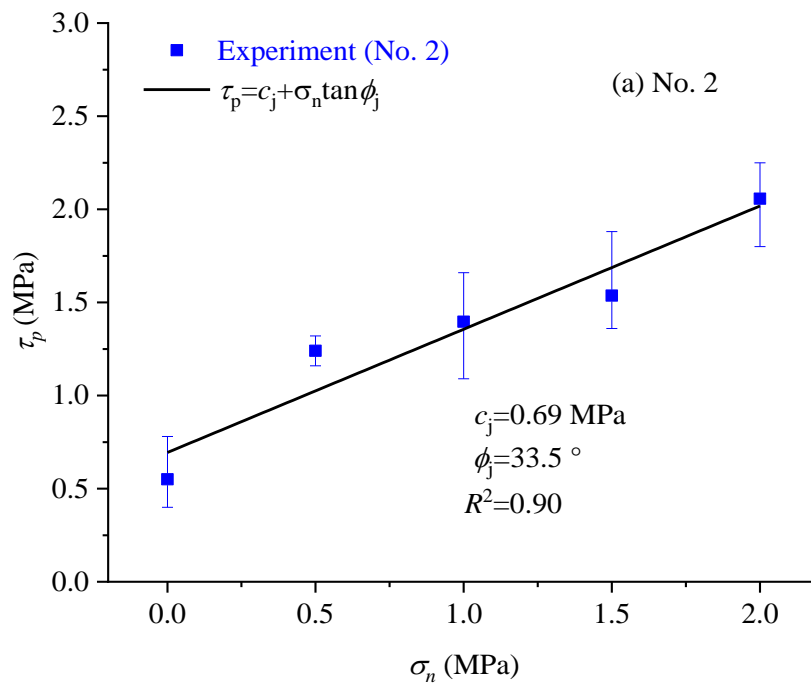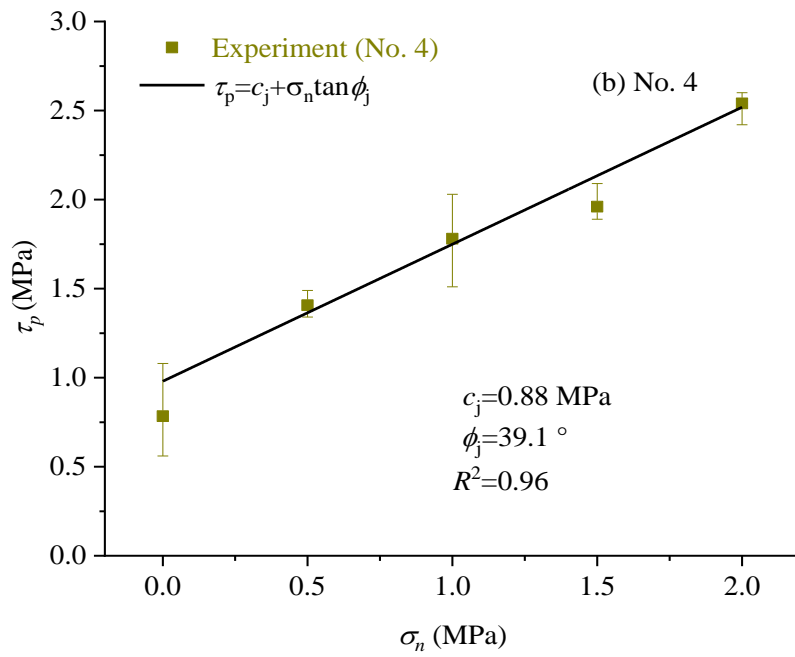
377
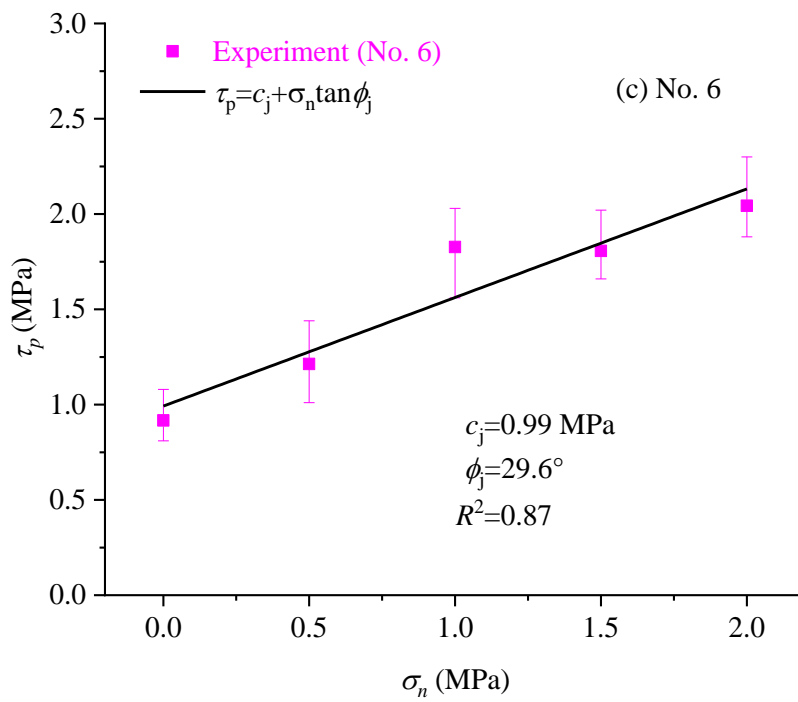
378
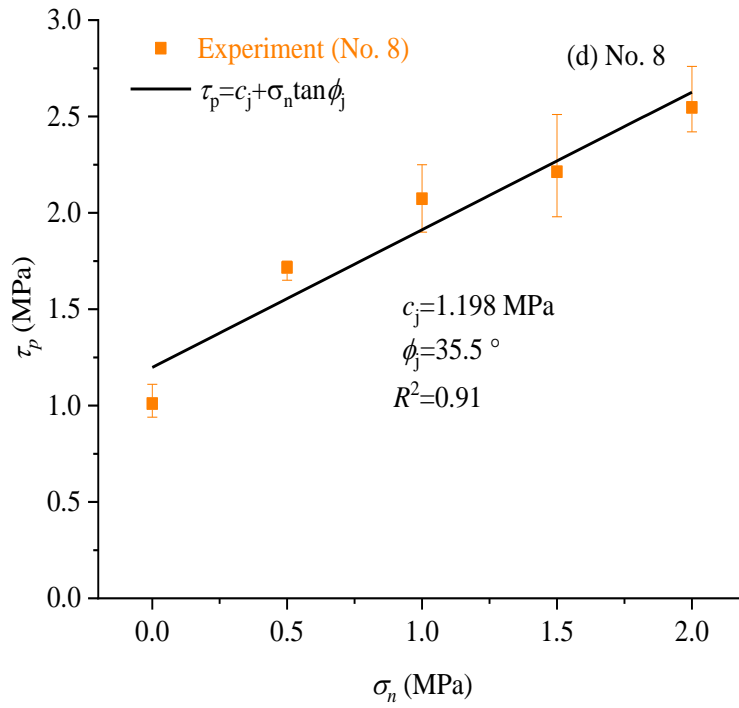
379
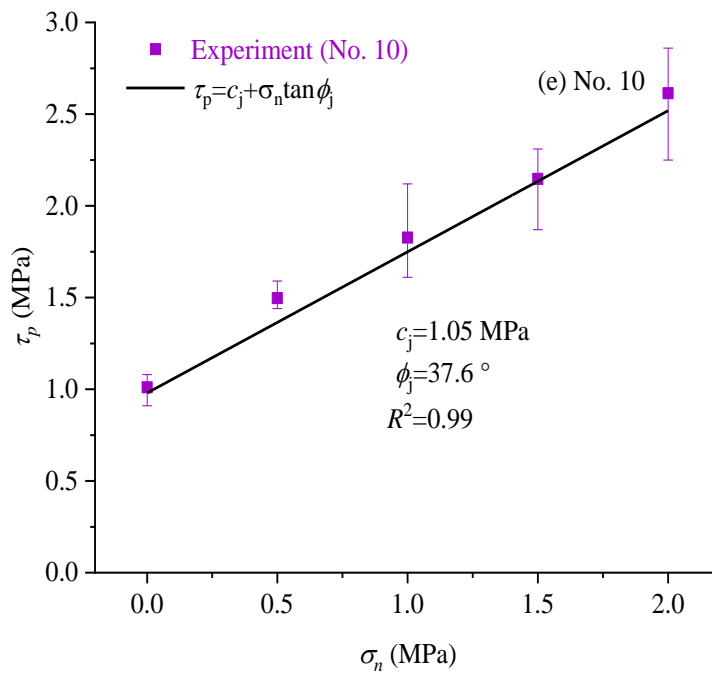
380

381 **Figure 17.** Effect of normal stress on the peak shear strength of ice-filled joints. Experimental condition: $T = $ -15 °C,

382 $v = 0.2$ mm/min and $d = 2$mm.

383
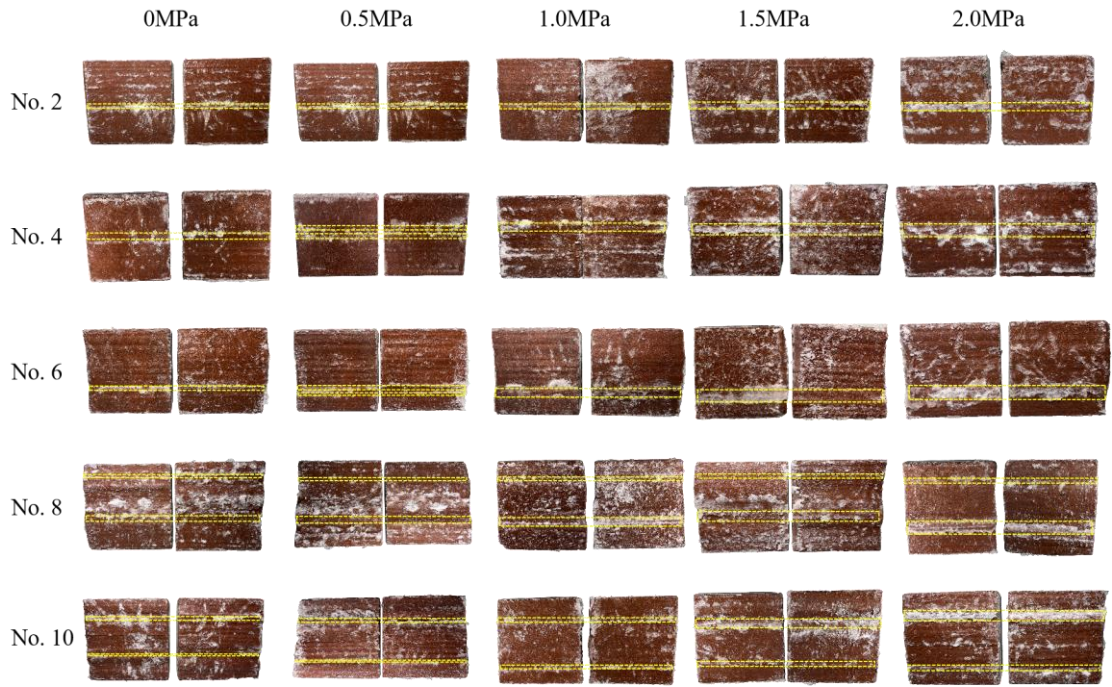
Figure 18. Aggregation of rupture ice under different normal stresses. Experimental condition: T = -15 °C, d = 2

mm and v = 0.2 mm/min. The yellow lines show the main aggregation of rupture ice.

386
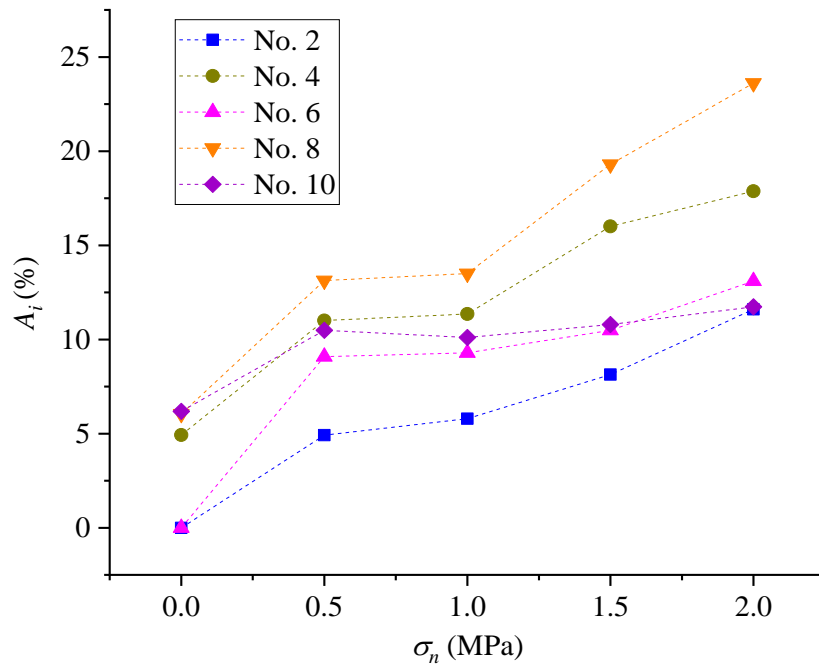
Figure 19. Aggregation area of rupture ice increases with increasing normal stress. Experimental condition: T = -

15 °C, d = 2 mm and v = 0.2 mm/min.

389
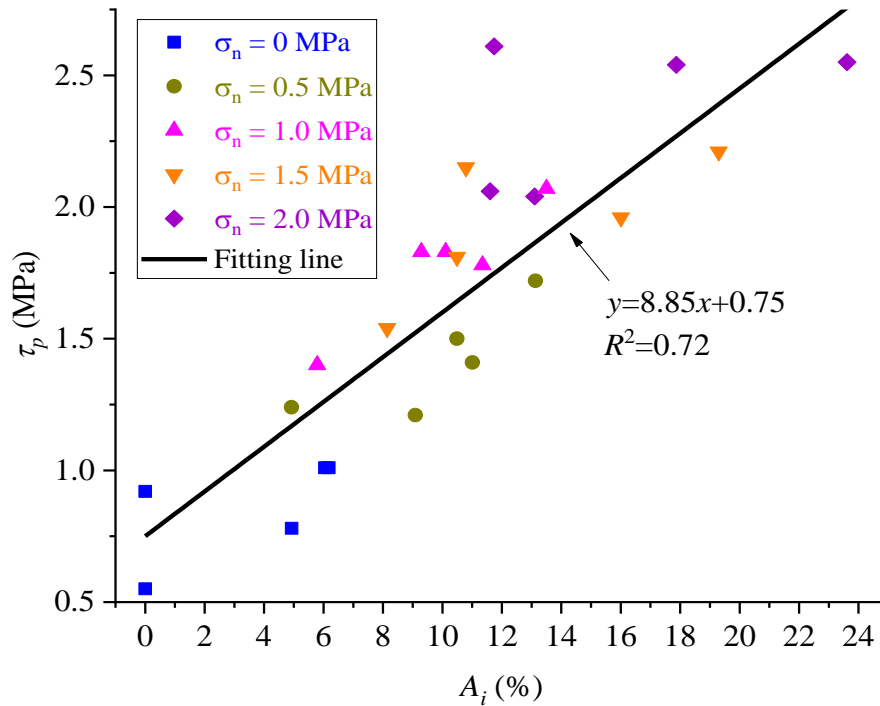
Figure 20. Peak shear strength linearly increases with increasing aggregation areas of rupture ice. Experimental

391   condition: T = -15 °C, d = 2 mm and v = 0.2 mm/min.

392   **4. Discussion**

393   **4.1 The warming degradation mechanism of ice-filled joints**

394   In this paper, the influence of freezing temperature, shear rate, joint opening and normal stress on the

395   shear strength of ice-filled joints in rock masses was comprehensively investigated by experiments. The

396   shear strength remarkably reduces with increasing freezing temperature, because the shear strengths of

397   solid ice and ice-rock interface decrease with increasing temperature. In order to deeply understand the

398   warming degradation mechanism of ice-filled joints, the shear strength of pure ice and ice-rock bonding

399   interface under different freezing temperatures also were tested in this study (Fig. 21).

400   The test results show that the shear strength of smooth ice-rock bonding interface is larger than that of

401   pure solid ice at the freezing temperature from -15 to -0.5 °C (Fig. 21a). It implies that the shear failure

402   should be inside the solid ice instead of ice-rock interface. When the freezing temperature increase from

403   -1 °C to -0.5 °C, the shear strengths of the ice-rock interface and the solid ice reduce very quickly. Jia et

404   al. (2015) also claimed the same change law of solid ice against the temperature.

405   However, the experimental results show that the shearing failure of many rough ice-filled joints at -0.5 °C

406   is the debonding of ice-rock interfaces (Figs. 6, 12, 13, 18). More shear experiments were carried out on

407   rough ice-rock interfaces with profiles of No. 4 and No. 8 on the same experimental condition ($\sigma_n = 0.5$

408   MPa, $v = 0.2$ mm/min). It shows that the shear strength of rock-ice-rock "sandwich" is a little larger than

409   that of ice-rock interface, although the change laws of them against temperature are very similar. Another

410   novel finding is that the shear strength of ice-rock interface is larger than the shear strength of solid ice

411   itself below -1 °C (Fig. 21b). Therefore, the shear failure below -1 °C displays the cracking of joint ice

412   instead of ice-rock interface, and some aggregation areas of rupture ice occur before large bulges (Figs.

413   6, 12, 13, 18). However, the shear strength of solid ice is larger than that of ice-rock interface above -

414   1 °C. This is the main reason for the shear failure of rough ice-filled joints along ice-rock interfaces at -

415   0.5 °C. The freezing temperature of -1 °C is the transition point of shear failure modes. Figure 22 presents

416   that the shear failure is along the ice-rock interface when the freezing temperature is approximate -0.5 °C,

417   however, the area of ice attached to the joints has a great increment with the decrement of freezing

418   temperature from -0.5 °C to -15 °C. It further illustrates that the shear strength of rough ice-rock interface

419   is larger than that of the solid ice below -5°C. Mamot et al. (2018) also found that the shear failure modes

420   of the smooth ice-filled joints changed from shearing cracking of joint ice to the debonding of ice-rock

421 interface when the freezing temperatures increased from -10 ℃ to -0.5 ℃. The smooth joints have a little

422 ability to resist the shear slide of ice-filled joints. Mamot et al. (2018) claimed that three shear failure

423 modes may arise between -5 ℃ to -1 ℃, including the debonding of ice-rock interface, shear cracking

424 of joint ice and their mixed mode. However, only the shear cracking of joint ice occurs at -5 ℃ to -1 ℃

425 in this study. Therefore, the joint roughness has an effect on the shear strength of ice-filled joints and the

426 shear failure modes.

427
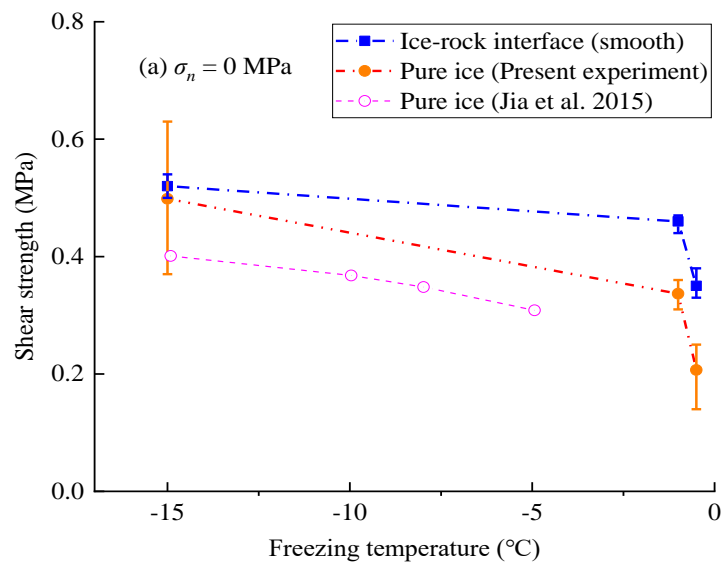
428
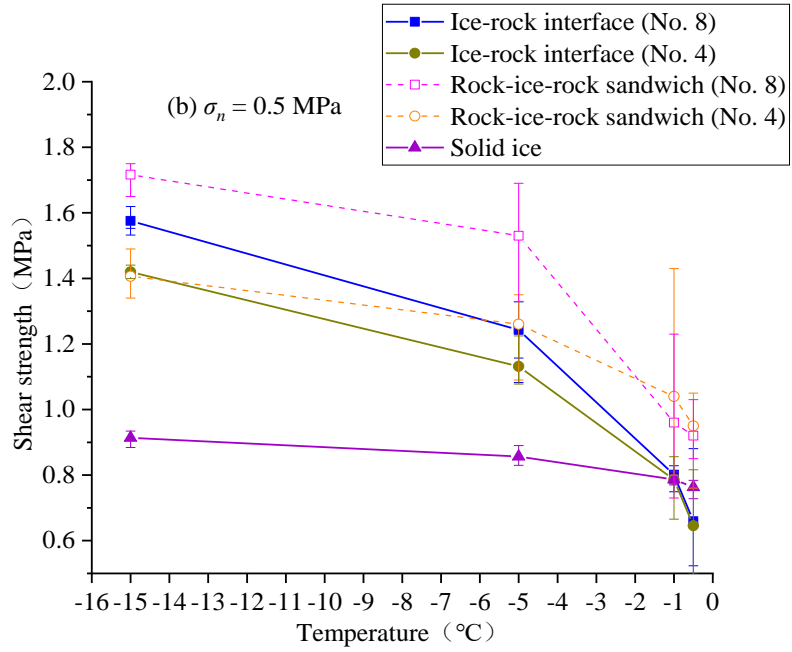
429 **Figure 21.** Influence of freezing temperature on the direct shear strength of ice and ice-filled joints. Experimental

430 condition: $v = 0.2$ mm/min.

431
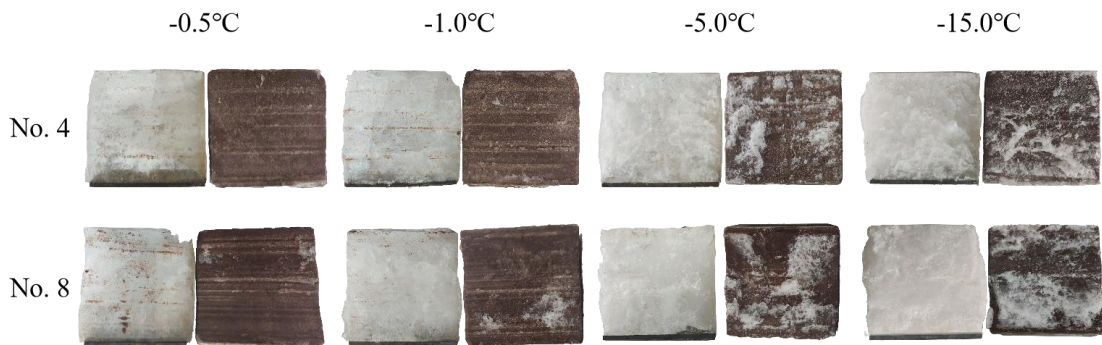
432 **Figure 22.** Shear failure characteristics of ice-rock interfaces under different temperatures. Experimental condition:

433 $v = 0.2$ mm/min, $\sigma_n = 0.5$ MPa.

434

435 **4.2 The coupled effect of joint roughness, opening and normal stress**

436 The shear strength of smooth ice-filled joints were investigated by Mamot et al. (2018). They found that

437 the shear strength of smooth ice-filled joints also linearly increases with decreasing temperatures.

438   Actually, the roughness is another important factor influencing the shear strength of ice-filled joints,

439   which can improve the ability to resist the shear slide of joints (Fig. 23). The shear strength of the No. 2

440   ice-filled joint is much smaller than that of No. 8 and No. 10 joints. For the profile of No. 2, the shear

441   strength of ice-filled joint is approximately equal to that of the solid ice when the normal stress is less

442   than 1.5 MPa, because the joint opening of 2 mm also is very close to the maximum height difference.

443   Therefore, the joint opening will determine the effect of joint roughness. However, the shear strength of

444   solid ice is much smaller compared with the shear strength of ice-filled joints when the normal stress is

445   2 MPa. It is observed that this normal stress has caused some vertical micro-cracks inside the solid ice.

446   For the ice-filled joints, the compression damage maybe not remarkable, because both the adhesion of

447   ice-rock interface and bulges will prevent the lateral expansion of solid ice under high normal stress. A

448   larger roughness may provide a much stronger confining effect on the lateral expansion. Although the

449   shear strength increases with increasing JRC number in general, the quantitative relationship between

450   them are hard to determine. Figure 5 shows that the change of shear strength against the JRC number is

451   fluctuating. A novel finding of this study is that the aggregation area of rupture ice before large bulges

452   can be well used to predict the shear strength of ice-filled joints. However, it should be noted that a new

453   index of roughness should be proposed in future research in order to build the shear strength model

454   considering joint roughness.

455   In addition, if the joint opening exceeds the critical value, the influence of joint roughness on the shear

456   strength of ice-filled joints will disappear. For example, when the thickness of joint ice exceeds 14 mm,

457   the shear strength of all the ice-filled joints is equal to the shear strength of infilled ice. Section 3.4 has

458   illustrated that the value of critical joint opening is depended on the maximum height different of the

459   joint, which need to study further.
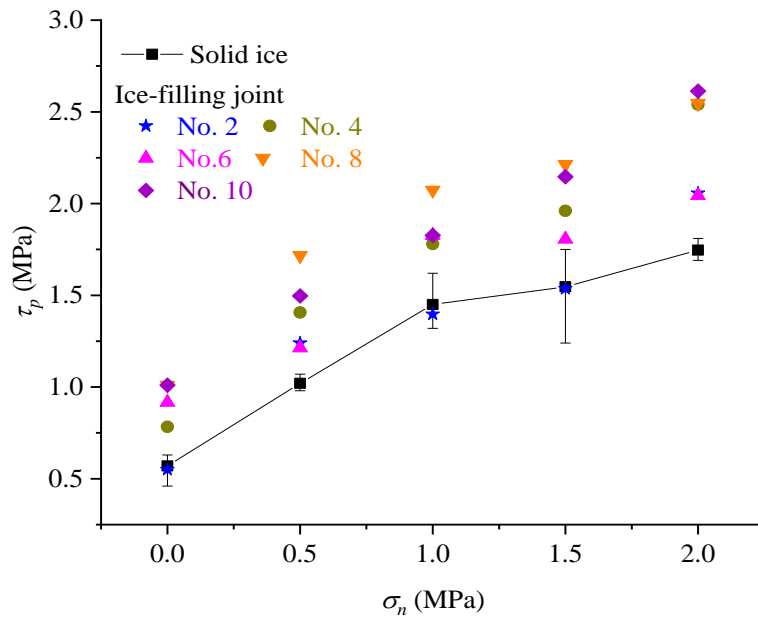
460

461   **Figure 23.** Shear failure characteristics of ice-rock interfaces under different normal stress. Experimental condition:

462   $v = 0.2$mm/min, $d = 2$ mm, $T = -15$ °C.

463

464   **4.3 Potential application for prediction of rock avalanches in a warming climate**

465   In recent years, there are many large rock avalanches occurred in the Alps. The rock avalanches that

466   occurred on the Brenva galcier, the Punta Thurwieser and the Drus are some of the recent examples,

467   which have strong impacts on the high mountain infrastructure stability and landscape evolution (Mamot

468   et al., 2018). The rock avalanches are related to the degradation of bedrock permafrost and ice-filled

469   joints. Our study shows that the peak shear strength of ice-filled joints increases with the increase of

470   roughness and normal pressure. This implies that the rockfall will be more stable with higher roughness

471   and normal pressure. In addition, when the joint openings increase, the peak shear strength will decrease,

472 and large joint openings will reduce the effect of joint roughness. The peak shear strength of ice-filled

473 joints decreases with the increase of freezing temperature. Moreover, when the freezing temperature is

474 close to 0 ℃, the pre-melting of ice-rock interface induced by the normal stress will cause a reduction of

475 bonding strength. This result can explain the phenomenon that the boundary of ice-filled joint between

476 frozen and unfrozen become unstable, especially in summer. The peak shear strength of ice-filled joints

477 decreases with the increase of shear rate. It is hard for the ice crystal to adjust to adapt the shear slip at

478 high shear rates so the rockfall may happen.

479 As the global temperature rises, collapse disasters of ice-filled rock mass caused by warming and thawing

480 often occur in permafrost regions. A constitutive model can be further constructed according to the

481 experiment results. Then combining with a numerical software, this constitutive model can be used to

482 predict the disaster of rock avalanches in the cold region in the future research. Although Mamot et al.

483 (2018) has established a constitutive model for joints, the constitutive model only considers temperature

484 and normal stress, however, the influence of the joint roughness, opening and shear rate is ignored.

485 Through our study, it is evidenced that the joint roughness, shear rate, joint opening and temperature are

486 physical quantities that must be considered in the constitutive model. A constitutive model including

487 these physical quantities will be proposed in our future research.

488 **5 Conclusions**

489 The following conclusions can be obtained in this study:

490 (1) The shear strength of ice-filled joints decreases with increasing temperature. The shear failure mode

491 change from shear rupture of joint ice to the debonding of ice-rock interface when the temperature

492 increases to -0.5 °C, because the bonding strength of ice-rock interface is less than that of solid ice at -

493 0.5 °C ($v = 0.2$ mm/min, $\sigma_n = 0.5$ MPa).

494 (2) The joint roughness can improve the shear strength of ice-filled joints, but it is related to the joint

495 opening and normal stress. The shear strength of ice-filled joints linearly increases with increasing the

496 aggregation area of rupture ice before noticeable bulges. However, the relationship between the JRC

497 index and the shear strength is not significant.

498 (3) The shear strength of ice-filled joints decreases with increasing joint opening. When the joint opening

499 increases from 2 mm to 14 mm, the aggregation of rupture ice gradually disappears and the shear strength

500 of ice-filled joint is equal to that of solid ice. A critical value of infilled thickness may exist, which need

501 further study.

502 (4) The shear strength of ice-filled joints decreases when the shear rate increase from 0.2 mm/min to 0.8

503 mm/min. The infilled ice may change from ductile to brittle failure with increasing shear rate. The

504 aggregation area of rupture ice also decreases while the brittle rupture phenomenon of joint ice is more

505 obvious as the shear rate increases.

506 (5) The shear strength of ice-filled joints linearly increases with increasing normal stress, which well

507 satisfies the Mohr-coulomb criterion. The aggregation area of rupture ice also increases with increasing

508 normal stress. In addition, the improvement of shear strength caused by the normal stress is much larger

509 for the ice-filled joints than the solid ice, because the bulges can prevent the lateral expansion of ice

510 under compression.

511   **Acknowledgements**

512   This work was supported by National Natural Science Foundation of China (Grant No. 42072300 and

513   No. 41702291), Project of Natural Science Foundation of Hubei Province (Grant No. 2021CFA094).

514   **Conflict of interest**

515   The authors declared that they have no conflicts of interest to this work.

516   **Reference**

517   Allen, S. and Huggel, C.: Extremely warm temperatures as a potential cause of recent high mountain

518   rockfall, Global. Planet. Change., 107, 59-69, https://doi.org/10.1016/j.gloplacha.2013.04.007, 2013.

519   Barton, N. and Choubey, V.: The shear strength of rock joints in theory and practice, J. Rock. Mech.

520   Geotech., 10, 1-54,https://doi.org/10.1007/BF01261801, 1977.

521   Bragov, A., Igumnov, L., Konstantinov, A., Lomunov, A., Filippov, A., Shmotin, Y., Didenko R. and

522   Krundaeva, A.: Investigation of strength properties of freshwater ice, EPJ Web of Conferences., 94,

523   01070, https://doi.org/10.1051/epjconf/20159401070, 2015.

524   Colucci, R. R. and Guglielmin, M.: Climate change and rapid ice melt: Suggestions from abrupt

525   permafrost degradation and ice melting in an alpine ice cave, Prog. Phys. Geog., 43, 561-573,

526   https://doi.org/10.1177/0309133319846056, 2019.

527   Davies, M. C., Hamza, O. and Harris, C.: The effect of rise in mean annual temperature on the stability

528   of   rock   slopes   containing   ice-filled   discontinuities,   Permafrost.   Periglac.,   12,   137-144,

529   https://doi.org/10.1002/ppp.378, 2001.

530 Davies, M. C., Hamza, O., Lumsden, B. W. and Harris, C.: Laboratory measurement of the shear strength

531 of ice-filled rock joints, Ann. Glaciol., 31, 463-467, https://doi.org/10.3189/172756400781819897, 2017.

532 Etzelmüller, B., Czekirda, J., Magnin, F., Duvillard, P. A., Ravanel, L., Malet, E., Aspaas A., Kristensen

533 L., Skrede I., Majala G. D., Jacobs B., LeinauerJ., Hauck C., Hilbich C., Böhme M., Hermanns R.,

534 Eriksen H., Lauknes T. R., Krautblatter M. and Westermann, S.: Permafrost in monitored unstable rock

535 slopes in Norway–new insights from temperature and surface velocity measurements, geophysical

536 surveying, and ground temperature modelling, Earth. Surf. Dynam., 10, 97-129,

537 https://doi.org/10.5194/esurf-10-97-2022, 2022.

538 Fukuzawa, T. and Narita, H.: An experimental study on the mechanical behavior of a depth hoar layer

539 under shear stress. Ph.D. thesis, Institute of Low Temperature Science, Hokkaido University, Japan, 5 p

540 p., 1993.

541 Gruber, S. and Haeberli, W.: Permafrost in steep bedrock slopes and its temperature-related

542 destabilization following climate change, J. Geophys. Res.-Earth., 112, F02S18,

543 https://doi.org/10.1029/2006JF000547, 2007.

544 Han, H. W., Jia, Q., Huang, W. F. and Li, Z. J.: Flexural strength and effective modulus of large

545 columnar-grained freshwater ice, J. Cold. Reg. Eng., 30, 04015005,

546 https://doi.org/10.1061/(ASCE)CR.1943-5495.0000098, 2016.

547   Hartmeyer, I., Delleske, R., Keuschnig, M., Krautblatter, M., Lang, A., Schrott, L. and Otto, J. C.: Current

548   glacier recession causes significant rockfall increase: the immediate paraglacial response of deglaciating

549   cirque walls, Earth. Surf. Dynam., 8, 729-751, https://doi.org/10.5194/esurf-8-729-2020, 2020.

550   Hilger, P., Hermanns, R. L., Czekirda, J., Myhra, K. S., Gosse, J. C. and Etzelmüller, B.: Permafrost as

551   a first order control on long-term rock-slope deformation in (Sub-) Arctic Norway, Quaternary. Sci. Rev.,

552   251, 106718, https://doi.org/10.1016/j.quascirev.2020.106718, 2021.

553   Huang, S. B., Yu, S. L., Ye, Y. H, Ye, Z. Y. and Cheng, A. P.: Pore structure change and physico-

554   mechanical properties deterioration of sandstone suffering freeze-thaw actions, Constr. Build. Mater.,

555   330, 127200, https://doi.org/10.1016/j.conbuildmat.2022.127200, 2022.

556   Huang, S. B., Wang, J., Liu, Y. Z., Tian, Q. and Cai, C.: Experimental investigation on crack coalescence

557   and strength loss of rock-like materials containing two parallel water-filled flaws under freeze-thaw.

558   Theor. Appl. Fract. Mec., S0167-8442(22), 00413-X, https://doi.org/10.1016/j.tafmec.2022.103669,

559   2022b.

560   Krautblatter, M., Funk, D., Günzel, F. K.: Why permafrost rocks become unstable: a rock-ice-mechanical

561   model in time and space, Earth. Surf. Proc. Land., 38, 876-887, https://doi.org/10.1002/esp.3374, 2012.

562   Krautblatter, M., Huggel, C., Deline, P. and Hasler, A.: Research perspectives on unstable high-alpine

563   bedrock permafrost: Measurement, modelling and process understanding, Permafrost. Periglac., 23, 80-

564   88, https://doi.org/10.1002/ppp.740, 2021.

565 Legay, A., Magnin, F. and Ravanel, L.: Rock temperature prior to failure: Analysis of 209 rockfall events

566 in the Mont Blanc massif (Western European Alps), Permafrost. Periglac., 32, 520-536,

567 https://doi.org/10.1002/ppp.2110, 2021.

568 Lou, X. N. and Wu, Y.: Influence of temperature and fiber content on direct shear properties of plain ic

569 e and fiber-reinforced ice, Cold. Reg. Sci. Technol., 194, 103458,

570 https://doi.org/10.1016/j.coldregions.2021.103458, 2021.

571 Luo, S., Li, C., Li, F., Wang, J. and Li, Z. G.: Ice crystallization in shear flows, J. Phys. Chem. C., 123,

572 21042-21049, https://doi.org/10.1021/acs.jpcc.9b06225, 2019.

573 Mamot, P., Weber, S., Eppinger, S. and Krautblatter, M.: A temperature-dependent mechanical model to

574 assess the stability of degrading permafrost rock slopes, Earth. Surf. Dynam., 9, 1125-1151,

575 https://doi.org/10.5194/esurf-9-1125-2021, 2021.

576 Mamot, P., Weber, S., Schröder, T. and Krautblatter, M.: A temperature-and stress-controlled failure

577 criterion for ice-filled permafrost rock joints, Cryosphere., 12, 3333-3353, https://doi.org/10.5194/tc-12-

578 3333-2018, 2018.

579 Matsuoka, N. and Murton, J.: Frost weathering: recent advances and future directions, Permafrost.

580 Periglac., 19, 195-210, https://doi.org/10.1002/ppp. 620, 195-210.

581 Petrovic, J. J.: Review mechanical properties of ice and snow, J. Mater. Sci., 38, 1-6,

582 https://doi.org/10.1023/A:1021134128038, 2003.

583 Ren, X. H.: Investigation on ductile-to-brittle transition behavior of ice, Ph.D. dissertation, Dalian

584 University of Technology, China, 64 pp, 2005.

585 Schulson, E. M. and Fortt, A. L.: Friction of ice on ice, J. Geophys. Res.-Sol. Ea., 117, B12204,

586 https://doi.org/10.1029/2012JB009219, 2012.

587 Shan, R. L., Bai, Y., Ju, Y., Han, T. Y., Dou, H. Y. and Li, Z. L.: Study on the triaxial unloading creep

588 mechanical properties and damage constitutive model of red sandstone containing a single ice-filled flaw,

589 Rock. Mech. Rock. Eng., 54, 833-855, https://doi.org/10.1007/s00603-020-02274-1, 2021.

590 Shen, Y. J., Yang, H. W., Xi, J. M., Yang, Y., Wang, Y. Z. and Wei, X.: A novel shearing fracture

591 morphology method to assess the influence of freeze-thaw actions on concrete-granite interface, Cold.

592 Reg. Sci. Technol., 169, 102900, https://doi.org/10.1016/j.coldregions.2019.102900, 2020.

593 Shugar, D. H., Jacquemart, M., Shean, D., Bhushan, S., Upadhyay, K., Sattar, A., Schwanghart, W.,

594 Mcbride, S., Van Wyk De Vries, M., Mergili, M., Emmer, A., Deschamps-Berger, C., Mcdonnell, M.,

595 Bhambri, R., Allen, S., Berthier, E., Carrivick, J. L., Clague, J. J., Dokukin, M., Dunning, S. A., Frey,

596 H., Gascoin, S., Haritashya, U. K., Huggel, C., Kääb, A., Kargel, J. S., Kavanaugh, J. L., Lacroix, P.,

597 Petley, D., Rupper, S., Azam, M. F., Cook, S. J., Dimri, A. P., Eriksson, M., Farinotti, D., Fiddes, J.,

598 Gnyawali, K. R., Harrison, S., Jha, M., Koppes, M., Kumar, A., Leinss, S., Majeed, U., Mal, S., Muhuri,

599 A., Noetzli, J., Paul, F., Rashid, I., Sain, K., Steiner, J., Ugalde, F., Watson, C. S. and Westoby, M. J.: A

600 massive rock and ice avalanche caused the 2021 disaster at Chamoli, Indian Himalaya, Science., 373,

601 300-306, 10.1126/science.abh4455, 2021.

602   Sinha, N. K.: Elasticity of natural types of polycrystalline ice, Cold. Reg. Sci. Technol., 17, 127-135,

603   https://doi.org/10.1016/S0165-232X(89)80003-5, 1989.

604   Walter, F., Amann, F., Kos, A., Kenner, R., Phillips, M., de Preux, A., Huss, M., Tognacca, C., Clinton,

605   J., Diehl, T. and Bonanomi, Y.: Direct observations of a three million cubic meter rock-slope collapse

606   with almost immediate initiation of ensuing debris flows, Geomorphology., 351, 106933,

607   https://doi.org/10.1016/j.geomorph.2019.106933, 2019.

608   Wang, C., Li, Y., Dai, F., Wu, G. N., Yin, F. T., Li, K. P. and Wang, K.: Experimental investigation on

609   mechanical properties and failure mechanism of rock-like specimens containing an arc-shaped ice-

610   filled flaw under uniaxial compression, Theor. Appl. Fract. Mec., 119, 103368,

611   https://doi.org/10.1016/j.tafmec.2022.103368, 2022.

612   Weber, S., Fäh, D., Beutel, J., Faillettaz, J., Gruber, S. and Vieli, A.: Ambient seismic vibrations in steep

613   bedrock permafrost used to infer variations of ice-fill in fractures, Earth. Planet. Sc. Lett., 501, 119-127,

614   https://doi.org/10.1016/j.epsl.2018.08.042, 2018.

615   Yang, Q. Q., Su, Z. M., Cheng, Q. G., Ren, Y. H. and Cai, F.: High mobility of rock-ice avalanches:

616   Insights from small flume tests of gravel-ice mixtures, Eng. Geol., 260, 105260,

617   https://doi.org/10.1016/j.enggeo.2019.105260, 2019.

618   Xu, D. P., Feng, X. T., Cui, Y. J.: A simple shear strength model for interlayer shear weakness zone. Eng.

619   Geol., 147, 114-123, http://dx.doi.org/10.1016/j.enggeo.2012.07.016, 2012.

620   Zhang, G. Z., Chen, G. Q., Xu, Z. X., Yang, Y. and Lin, Z. H.: Crack failure characteristics of different

621   rocks under the action of frost heaving of fissure water, Front. Earth. Sc.-Switz., 8, 13,

622   https://doi.org/10.3389/feart.2020.00013, 2020.

623   Zhao, Y. L., Zhang, L. Y., Asce, F., Wang, W. J., Liu, Q., Tang, L. M. and Cheng, G. M.: Experimental

624   Study on Shear Behavior and a Revised Shear Strength Model for Infilled Rock Joints, Int. J. Geomech.,

625   20(9), 04020141, 10.1061/(ASCE)GM.1943-5622.0001781, 2020.

626   Zhao, Z. H., Yang, J., Zhou, D. and Chen, Y. F.: Experimental investigation on the wetting-induced

627   weakening of sandstone joints, Eng. Geol., 225, 61-67, https://doi.org/10.1016/j.enggeo.2017.04.008,

628   2017.